Temporal decay of coherently optically injected charge and spin currents due to carrier–LO-phonon and carrier-carrier scattering

H. T. Duc,[1,2] Q. T. Vu,[1,3] T. Meier,[1] H. Haug,[4] and S. W. Koch[1]
[1]*Department of Physics and Material Sciences Center, Philipps University, Renthof 5, D-35032 Marburg, Germany*
[2]*Ho Chi Minh City Institute of Physics, Viet Nam Center for Natural Science and Technology, 1 Mac Dinh Chi, Ho Chi Minh City, Vietnam*
[3]*Faculty of Physics, University of Natural Sciences, Nguyen Van Cu 227, District 5, Ho Chi Minh City, Vietnam*
[4]*Institut für Theoretische Physik, Johann Wolfgang Goethe–Universität Frankfurt, Max-von-Laue-Strasse 1, D-60438 Frankfurt, Germany*

(Received 28 June 2006; revised manuscript received 28 August 2006; published 26 October 2006)

The coherent ultrafast optical injection and the temporal evolution of charge and spin currents in semiconductors is analyzed using a microscopic many-body theory. The approach is based on the semiconductor Bloch equations and includes light-field-induced intraband and interband excitations, excitonic effects, and carrier–LO-phonon and carrier-carrier scattering processes. The relaxation effects are treated both in the second Born-Markov approximation and on the level of quantum kinetic theory including memory effects. The dynamics of the charge and spin currents is evaluated numerically for a one-dimensional model system. The dependence of the currents and their decay on the temperature, the excitation intensities, and the frequencies of the incident light fields is discussed. Whereas the overall decay dynamics is described well within the Markov approximation, the quantum kinetic theory predicts additional oscillatory signatures in the current transients.

DOI: 10.1103/PhysRevB.74.165328 PACS number(s): 72.25.Fe, 42.65.−k, 72.25.Rb

I. INTRODUCTION

The coherent ultrafast generation of photocurrents in semiconductors and semiconductor heterostructures by sequences of optical laser pulses has attracted a great deal of attention recently.[1–17] In particular, it has been predicted[2] and observed[3] that it is possible to generate photocurrents in semiconductors via the excitation with two light fields with frequencies ω and 2ω, which satisfy $2\hbar\omega > E_{\mathrm{gap}} > \hbar\omega$, where E_{gap} is the band-gap energy. In this scheme, the valence- and conduction-band states are coupled by both one- and two-photon transitions, which allows one to coherently control the photoexcitations. The interference between interband and intraband transitions may lead to photoexcited electronic distributions which are not symmetric in k space, i.e., they correspond to a nonvanishing current. The generated photocurrents depend sinusoidally on the relative phase between the two incident fields. For the case of disordered semiconductors, it has been predicted that sequences of temporally delayed excitation pulses may lead to current echoes,[6,7] however this phenomenon has not yet been observed experimentally.

The interference of the ω and 2ω fields can be used to excite charge currents for the case of linear parallel polarization. Due to the dependence of the transition matrix elements on the spin, however, for linear perpendicular polarization directions of the incident pulses, the same interference scheme can be used to generate spin currents.[4,11] In such a situation, electrons with opposite spin predominantly move into opposite directions such that no effective charge but just the spin is transported. These spin currents have been observed recently.[8–10] They could be of interest for future applications in the area of spintronics.[18,19]

Whereas the formulation of the current generation in terms of nonlinear optical susceptibilities is very useful in determining the existence and strength of coherent photocurrents for various crystal symmetries and excitation geometries,[2,11] a detailed microscopic understanding of the temporal evolution of these currents requires the evaluation of dynamic equations. Sets of Bloch equations for the relevant intraband and interband transitions and populations have been successfully used to describe the coherent generation and dynamics of the currents.[6,7,13,15] Excitonic effects have been shown to lead to phase shifts of the photo- and spin currents in bulk semiconductors,[14] and interferences between optically allowed and forbidden excitons in quantum wires can be used to generate oscillating photocurrents.[15]

Only a little knowledge is available on the temporal decay of the coherent photocurrents, which is modeled by phenomenological decay times in most of the existing publications. However, the relaxation of the electronic current by the scattering with LO phonons has been analyzed[5] and some results on the decay of the spin current by carrier-carrier scattering in bulk GaAs have been obtained by considering a rather simple model.[20] It has been shown recently that carrier-carrier scattering processes may lead to a more rapid decay of the spin current as compared to that of the charge current.[16] This result has been obtained without taking any spin relaxation mechanisms[21–23] into account and is a consequence of the momentum-exchanging but spin-conserving Coulomb scattering between the carriers with opposite spin. Therefore, the explanation of the enhanced damping of the photogenerated spin current is similar to the spin Coulomb drag that has been found in studies of spin-polarized transport.[24]

In this paper, we analyze the dynamical generation and the decay of charge and spin currents using a microscopic many-body theory that is based on the semiconductor Bloch equations (SBE), i.e., the equations of motion for the optical polarization and the carrier populations.[25–27] This coupled set of equations nonperturbatively includes light-field-induced intraband and interband excitations. The coherent part of the SBE furthermore contains the first-order Hartree-Fock Coulomb effects, i.e., excitonic effects and Coulombic nonlinearities due to energy and field renormalization.[25–27] In order to be able to describe besides the coherent dynamics of the currents also the subsequent temporal decay, incoherent scattering processes are also considered. Therefore, the coherent SBE are supplemented by collision contributions that describe carrier–LO-phonon and carrier-carrier scattering. These processes are known to dominate the ultrafast relaxation and dephasing dynamics of photoexcited semiconductors. In this paper, we describe these terms either on the level of a second-order Born-Markov approximation[25–29] or at the level of non-Markovian quantum-kinetic theory.[30] We investigate the decay of the charge and spin currents induced by these scattering contributions. Further processes, in particular spin relaxation mechanisms,[19,21–23] are not taken into account by our present two-band model. Thus the results reported here are apply to situations in which the damping of the photocurrents is mainly caused by the energy relaxation of the photogenerated nonequilibrium carrier distributions. The model used here can be extended to incorporate further bands and spin relaxation mechanisms. This will, however, largely increase the numerical requirements. It can be expected that the enhancement of the damping of the photogenerated spin current as compared to that of the charge current will increase if spin relaxation processes are relevant.

Using the Markovian approximation in the evaluation of the scattering terms is valid in the long-time regime, where the energy conservation for each completed collision strictly holds. This approximation, however, fails to describe some characteristic features on the ultrashort time scale since quantum kinetic effects, i.e., the finite duration of collisions, are neglected. In a short-time interval, the energy is not conserved in a single scattering event and the system has a memory of its previous states. In order to investigate the influence of these effects, we apply the quantum kinetic approach[30] and analyze the Coulomb and LO-phonon relaxation dynamics on ultrafast time scales.

We have structured this paper such that the following Sec. II presents the Hamiltonian and the coherent part of the SBE. The collision contributions as they arise in the second Born-Markov approximation and in the quantum-kinetic theory are given in Appendix A. In Appendix B we present a third-order expansion of the SBE which systematically shows the generation of the optically induced currents.

Due to the extensive numerics involved with the solution of our coupled system of equations and in order to be able to perform a systematic analysis of the relaxation dynamics with and without Markov approximations, we consider here a relatively simple model system for a one-dimensional quantum wire with two parabolic bands using GaAs parameters, see Sec. III. Numerical results on the dynamical evolution of the distribution functions and the charge and spin currents are presented in Sec. IV. Of particular importance is the dependence of the currents and their decay on the temperature, the excitation intensity, and the frequency of the incident light field. Furthermore, it is shown that the overall decay of the currents is basically correctly described by Markovian calculations. However, quantum-kinetic memory effects may lead to additional oscillatory signatures in the current transients. Our most important results are summarized in the concluding Sec. V.

II. THEORY

We subdivide the Hamiltonian of our interacting many-body system into five individual contributions,[25,26,34]

$$H = H_{\text{band structure}} + H_{\text{light matter}} + H_{\text{Coulomb}} + H_{\text{phonon}} + H_{\text{carrier phonon}}. \tag{1}$$

In the following, we consider the spin-degenerate lowest conduction bands and the highest heavy-hole valence bands, which are denoted by c and v, respectively. The two spin directions are labeled by $\sigma=\uparrow,\downarrow$. The electronic single-particle energy is given by

$$H_{\text{band structure}} = \sum_{\lambda\sigma\mathbf{k}} \epsilon_{\lambda\mathbf{k}} a^{\dagger}_{\lambda\sigma\mathbf{k}} a_{\lambda\sigma\mathbf{k}}, \tag{2}$$

where $\varepsilon_{\lambda\mathbf{k}}$ is the band structure and $a^{\dagger}_{\lambda\sigma\mathbf{k}}$ ($a_{\lambda\sigma\mathbf{k}}$) is the creation (annihilation) operator of an electron with momentum $\mathbf{k}$ and spin σ in the band $\lambda=c,v$. The light-matter interaction is described semiclassically as

$$H_{\text{light matter}} = -\mathbf{E}(t)\cdot \sum_{\lambda\lambda'\sigma\sigma'\mathbf{k}\mathbf{k}'} \mathbf{d}^{\lambda\lambda'}_{\sigma\sigma'\mathbf{k}\mathbf{k}'} a^{\dagger}_{\lambda\sigma\mathbf{k}} a_{\lambda'\sigma'\mathbf{k}'}. \tag{3}$$

Here, $\mathbf{E}(t)$ is the electric field and

$$\mathbf{d}^{\lambda\lambda'}_{\sigma\sigma'\mathbf{k}\mathbf{k}'} = e\mathbf{r}^{\lambda\lambda'}_{\sigma\sigma\mathbf{k}} \delta_{\sigma\sigma'}\delta(\mathbf{k}-\mathbf{k}') + ie\delta_{\sigma\sigma'}\delta_{\lambda\lambda'}\nabla_{\mathbf{k}}\delta(\mathbf{k}-\mathbf{k}') \tag{4}$$

is the dipole matrix element where $\mathbf{r}^{\lambda\lambda'}_{\sigma\sigma\mathbf{k}}$ describes optical interband transitions and $\nabla_{\mathbf{k}}$ is the intraband acceleration.[31–35] The many-body Coulomb interaction between the carriers reads

$$H_{\text{Coulomb}} = \frac{1}{2}\sum_{\lambda\lambda'\sigma\sigma'\mathbf{k}\mathbf{k}'\mathbf{q}\neq 0} V_{\mathbf{q}} a^{\dagger}_{\lambda\sigma\mathbf{k}+\mathbf{q}} a^{\dagger}_{\lambda'\sigma'\mathbf{k}'-\mathbf{q}} a_{\lambda'\sigma'\mathbf{k}'} a_{\lambda\sigma\mathbf{k}}, \tag{5}$$

where $V_{\mathbf{q}}$ is the Coulomb matrix element. The energy of the phonon system is given by

$$H_{\text{phonon}} = \sum_{\mathbf{q}} \hbar\omega_{\mathbf{q}}\left(b^{\dagger}_{\mathbf{q}} b_{\mathbf{q}} + \frac{1}{2}\right). \tag{6}$$

Here, $b^{\dagger}_{\mathbf{q}}$ ($b_{\mathbf{q}}$) creates (annihilates) a phonon with wave vector $\mathbf{q}$ and energy $\hbar\omega_{\mathbf{q}}$. The carrier-phonon interaction is described by

$$H_{\text{carrier phonon}} = \sum_{\lambda\sigma\mathbf{k}\mathbf{q}} g_{\mathbf{q}} a^{\dagger}_{\lambda\sigma\mathbf{k}+\mathbf{q}} a_{\lambda\sigma\mathbf{k}} (b_{\mathbf{q}} + b^{\dagger}_{-\mathbf{q}}), \tag{7}$$

where the matrix element $g_{\mathbf{q}}$ determines the coupling strength.

The dynamical optoelectronic response is analyzed using the Heisenberg equations of motion for the carrier populations $n^e_{\sigma\mathbf{k}}=\langle a^\dagger_{c\sigma\mathbf{k}}a_{c\sigma\mathbf{k}}\rangle$ and $n^h_{\sigma\mathbf{k}}=1-\langle a^\dagger_{v\sigma\mathbf{k}}a_{v\sigma\mathbf{k}}\rangle$ and the interband polarization $p_{\sigma\mathbf{k}}=\langle a^\dagger_{v\sigma\mathbf{k}}a_{c\sigma\mathbf{k}}\rangle$. The resulting SBE read[25,26,31–34]

$$\frac{d}{dt}n^e_{\sigma\mathbf{k}}=-2\,\mathrm{Im}(\Omega^R_{\sigma\mathbf{k}}p^*_{\sigma\mathbf{k}})-\frac{e}{\hbar}\mathbf{E}(t)\cdot\nabla_{\mathbf{k}}n^e_{\sigma\mathbf{k}}+\left.\frac{d}{dt}n^e_{\sigma\mathbf{k}}\right|_{\mathrm{coll}}, \tag{8}$$

$$\frac{d}{dt}n^h_{\sigma\mathbf{k}}=-2\,\mathrm{Im}(\Omega^R_{\sigma\mathbf{k}}p^*_{\sigma\mathbf{k}})-\frac{e}{\hbar}\mathbf{E}(t)\cdot\nabla_{\mathbf{k}}n^h_{\sigma\mathbf{k}}+\left.\frac{d}{dt}n^h_{\sigma\mathbf{k}}\right|_{\mathrm{coll}}, \tag{9}$$

$$\frac{d}{dt}p_{\sigma\mathbf{k}}=-\frac{i}{\hbar}(\varepsilon^e_{\sigma\mathbf{k}}+\varepsilon^h_{\sigma\mathbf{k}})p_{\sigma\mathbf{k}}-i(n^e_{\mathbf{k}}+n^h_{\mathbf{k}}-1)\Omega^R_{\sigma\mathbf{k}}$$
$$-\frac{e}{\hbar}\mathbf{E}(t)\cdot\nabla_{\mathbf{k}}p_{\sigma\mathbf{k}}+\left.\frac{d}{dt}p_{\sigma\mathbf{k}}\right|_{\mathrm{coll}}, \tag{10}$$

where

$$\Omega^R_{\sigma\mathbf{k}}=\frac{1}{\hbar}\left[e\mathbf{r}^{cv}_{\sigma\sigma\mathbf{k}}\cdot\mathbf{E}(t)+\sum_{\mathbf{q}\neq\mathbf{0}}V_{\mathbf{q}}p_{\sigma\mathbf{k}+\mathbf{q}}\right] \tag{11}$$

is the generalized Rabi frequency and

$$\varepsilon^e_{\sigma\mathbf{k}}=\epsilon_{c\mathbf{k}}-\sum_{\mathbf{q}\neq\mathbf{0}}V_{\mathbf{q}}n^e_{\sigma\mathbf{k}+\mathbf{q}},\quad \varepsilon^h_{\sigma\mathbf{k}}=-\epsilon_{v\mathbf{k}}-\sum_{\mathbf{q}\neq\mathbf{0}}V_{\mathbf{q}}n^h_{\sigma\mathbf{k}+\mathbf{q}} \tag{12}$$

are the renormalized electron and hole energies. The terms written explicitly in Eqs. (8)–(10) are the ones arising in the time-dependent Hartree-Fock approximation for the Coulomb interaction. All contributions beyond this level are denoted by $|_{\mathrm{coll}}$. These *collision* terms, which arise as a consequence of the carrier-phonon and the carrier-carrier Coulomb interaction, are given in Appendix A. Since the light-matter and the carrier-phonon interactions are diagonal in the spin, Eqs. (8)–(10) describe within the time-dependent Hartree-Fock scheme a system of two uncoupled two-band situations characterized by the spin index $\sigma=\uparrow,\downarrow$. These optically isolated subsets are, however, coupled via Coulombic many-body correlations, i.e., the carrier-carrier scattering processes described in Appendix A.

Equations similar to Eqs. (8)–(10), however without inclusion of the spin degree of freedom, have been used already in Refs. 31–34 to describe the optoelectronic response of semiconductor superlattices in the presence of static and terahertz fields applied in the growth direction. In those studies, the optical fields were considered solely to generate interband transitions via the terms proportional to $\mathbf{E}(t)\cdot\mathbf{r}^{cv}_{\sigma\sigma\mathbf{k}}$, whereas the static and terahertz fields led to the intraband acceleration via the $\mathbf{E}(t)\cdot\nabla_{\mathbf{k}}$ terms. Such a distinction between rapidly oscillating and static or slowly oscillating fields was useful in order to apply the rotating-wave approximation when solving the SBE. In our present investigations, however, we are interested in describing the optical generation of currents by the interference of optical fields with frequencies ω and 2ω which fulfill $\hbar\omega<E_{\mathrm{gap}}<2\hbar\omega$, i.e., by two fields of comparable frequency. Therefore, the previously made simplification is not possible and instead the total field has to be considered for both the intraband and interband excitations. The results presented in Sec. IV are obtained by numerical integration of the SBE without invoking the rotating-wave approximation, i.e., by using a very small time step that resolves the optical oscillation period of the laser pulses. When solving Eqs. (8)–(10), it is, however, still possible to treat the intraband acceleration exactly by introducing a time-dependent frame according to[31–34]

$$\mathbf{k}(t)=\mathbf{k}(t=0)+\frac{e}{\hbar}\int^t dt'\mathbf{E}(t'), \tag{13}$$

i.e., the wave vector satisfies the acceleration theorem

$$\frac{d}{dt}\mathbf{k}(t)=\frac{e}{\hbar}\mathbf{E}(t). \tag{14}$$

Besides excitonic effects and the scattering terms, Eqs. (8)–(10) include nonperturbatively intraband and interband excitations induced by homogeneous electric fields. This allows us to study the dependence of the optoelectronic response on the intensity of the incident light fields. If one assumes that the incident fields are weak, it is justified to solve Eqs. (8)–(10) perturbatively in the light-matter interaction. In Appendix B, it is outlined how the SBE presented here can be limited to describe the generation of coherent photoinduced currents arising in third order in the light field.

The time-dependent polarizations and populations are obtained by solving Eqs. (8)–(10) including the scattering terms. The electron and hole populations $n^{e,h}_{\sigma\mathbf{k}}$ determine the dynamics of the charge and spin current densities, which are evaluated by computing

$$\mathbf{J}=e\sum_{\sigma\mathbf{k}}\mathbf{v}^c n^e_{\sigma\mathbf{k}}-e\sum_{\sigma\mathbf{k}}\mathbf{v}^v n^h_{\sigma\mathbf{k}}, \tag{15}$$

$$\mathbf{S}=\frac{\hbar}{2}\sum_{\sigma\mathbf{k}}\sigma\mathbf{v}^c n^e_{\sigma\mathbf{k}}-\frac{\hbar}{2}\sum_{\sigma\mathbf{k}}\sigma\mathbf{v}^v n^h_{\sigma\mathbf{k}}, \tag{16}$$

where $\mathbf{v}^\lambda=\nabla_{\mathbf{k}}\epsilon_{\lambda\mathbf{k}}/\hbar$ is the group velocity. In the effective-mass approximation, the group velocity is given by $\mathbf{v}^\lambda=\hbar\mathbf{k}/m_\lambda$.

III. ONE-DIMENSIONAL QUANTUM WIRE MODEL SYSTEM

If the electronic band structure is symmetric in k, the coherent generation of currents is due to material excitations that are not symmetric in k space. In such situations, solutions of Eqs. (8)–(10) beyond the rotating-wave approximation and including the scattering contributions are numerically quite demanding. Therefore, we limit the present analysis to a one-dimensional model system of a GaAs quantum wire with parabolic spin-degenerate valence and conduction bands. The electronic band structure is described by

$$\epsilon_{\lambda k_x}=\frac{\hbar^2k_x^2}{2m_\lambda}\pm\frac{E_{\mathrm{gap}}}{2}, \tag{17}$$

with $m_c=0.067m_0$, $m_v=-0.457m_0$, where m_0 is the free-electron mass, and $E_{\mathrm{gap}}=1.5$ eV.

In order to be able to analyze both charge and spin currents, the interband matrix elements $\mathbf{r}^{\lambda\lambda'}_{\sigma\sigma' k_x}$ are taken as

$$\mathbf{r}^{cv}_{\uparrow\uparrow k_x} = r_{cv}(1,i,0), \quad \mathbf{r}^{cv}_{\downarrow\downarrow k_x} = r_{cv}(1,-i,0), \tag{18}$$

with r_{cv}=3 Å and vanish for all other indices. We thus use the same circularly polarized dipole matrix elements that describe heavy-hole to conduction-band transitions in quantum wells close to the Γ point. This allows us to model charge and spin current generation using the same excitation configurations as in quantum wells. With regard to the decay of charge and spin currents, it has been shown that the results obtained within this one-dimensional model system are qualitatively similar to much more time-consuming two-dimensional calculations.[16]

The effective one-dimensional Coulomb potential in real space is given by[25]

$$V^{1\mathrm{D}}(z) = \frac{e^2}{\epsilon_\infty} \frac{1}{|z| + b}. \tag{19}$$

Here, the regularization parameter b is taken as $0.3a_0$, where a_0 is the three-dimensional exciton Bohr radius, and the dielectric constant is $\epsilon_\infty = 10.92$. In k space, the Coulomb potential is

$$V_q^{1\mathrm{D}} = 2\frac{e^2}{\epsilon_\infty}\left[\left(\frac{\pi}{2} - \mathrm{Si}(bq)\right)\sin(bq) - \mathrm{Ci}(bq)\cos(bq)\right], \tag{20}$$

where Si(x) and Ci(x) are the sine and cosine integrals, respectively.

The coupling of the electrons and holes to dispersionless LO phonons is described by the Fröhlich relation

$$g_q^2 = \frac{\hbar\omega_{\mathrm{LO}} V_q}{2}\left(1 - \frac{\epsilon_\infty}{\epsilon_0}\right). \tag{21}$$

Here, we use $\hbar\omega_{\mathrm{LO}}$=36 meV and ϵ_0=12.9.

The incident electric field consists of a superposition of two pulses with frequencies ω and 2ω, i.e.,

$$\mathbf{E}(t) = \mathbf{E}_\omega(t) + \mathbf{E}_{2\omega}(t). \tag{22}$$

The two fields are taken to be linearly polarized here and are given by

$$\mathbf{E}_\nu(t) = \mathbf{e}_\nu A_\nu (e^{-t^2/\tau_L^2} e^{-i\nu t - i\phi_\nu} + \mathrm{c.c.}). \tag{23}$$

In Eq. (23), $\mathbf{e}_\nu$ denotes the polarization direction, A_ν is the amplitude, and ϕ_ν is the phase of the field of frequency $\nu = \omega$ and 2ω, respectively. Both frequency components are considered as Gaussian-shaped pulses with a duration determined by τ_L. For the case in which both field components are linearly polarized in the x direction, i.e., $\mathbf{e}_\omega = \mathbf{e}_{2\omega} = \mathbf{e}_x$, the photoexcitation produces a pure charge current since the two spin systems are excited identically. For the case of linear perpendicularly polarized pulses, i.e., $\mathbf{e}_\omega = \mathbf{e}_x$ and $\mathbf{e}_{2\omega} = \mathbf{e}_y$, a pure spin current with no accompanying charge current is generated.

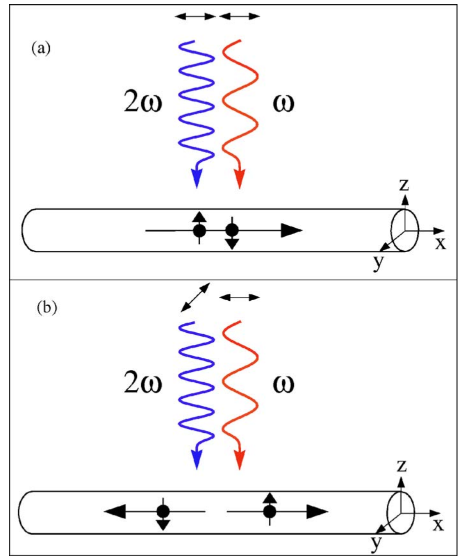

FIG. 1. (Color online) Schematic illustration of the excitation of the photocurrents with linearly polarized ω and 2ω fields. (a) When the polarization directions of the two fields are parallel and polarized along the direction of the quantum wire, i.e., $\mathbf{e}_\omega = \mathbf{e}_{2\omega} = \mathbf{e}_x$, a pure charge current J is generated. (b) When the two fields are perpendicularly polarized with $\mathbf{e}_\omega = \mathbf{e}_x$ and $\mathbf{e}_{2\omega} = \mathbf{e}_y$, a pure spin current S is generated.

IV. NUMERICAL RESULTS

In this section, we present results obtained by numerically solving the SBE, i.e., Eqs. (8)–(10), including carrier–LO-phonon and carrier-carrier scattering for the model system described in Sec. III. In Sec. IV A, we first analyze the excitation and decay of the charge and spin currents for the case in which the scattering terms are treated on the second Born-Markov level. Then in Sec. IV B, we discuss the results of our non-Markovian quantum kinetic calculations.

A. Charge and spin current dynamics at the Born-Markov level

The excitation geometries allowing for the generation of charge and spin currents are shown in Fig. 1. To excite a charge current J, both electric fields with frequencies ω and 2ω are polarized in the x direction, i.e., their polarization directions are $\mathbf{e}_\omega = \mathbf{e}_{2\omega} = \mathbf{e}_x$ in Eq. (23). A spin current S is injected by two cross-linearly-polarized pulses, where the ω pulse is polarized along x and the 2ω pulse is polarized in the y direction, i.e., $\mathbf{e}_\omega = \mathbf{e}_x$ and $\mathbf{e}_{2\omega} = \mathbf{e}_y$. The dynamics of the charge and spin currents are evaluated from the time-dependent populations using Eqs. (15) and (16), respectively.

The excitation conditions used in the following describe situations in which typically $2\hbar\omega$ is several excitonic binding energies above the band gap. Therefore, the phase shifts due to excitonic effects,[14] which are included in our analysis, are rather small. The charge and spin currents both depend sinusoidally on the phase difference between the ω and 2ω fields. In order to obtain a large current, we are guided by the phase dependence of the currents, which, without excitonic phase shifts, is given by $J \propto \sin(\phi_{2\omega} - 2\phi_\omega)$ and $S \propto \cos(\phi_{2\omega} - 2\phi_\omega)$.[3,8,10,11] Therefore, we use in our numerical calcula-

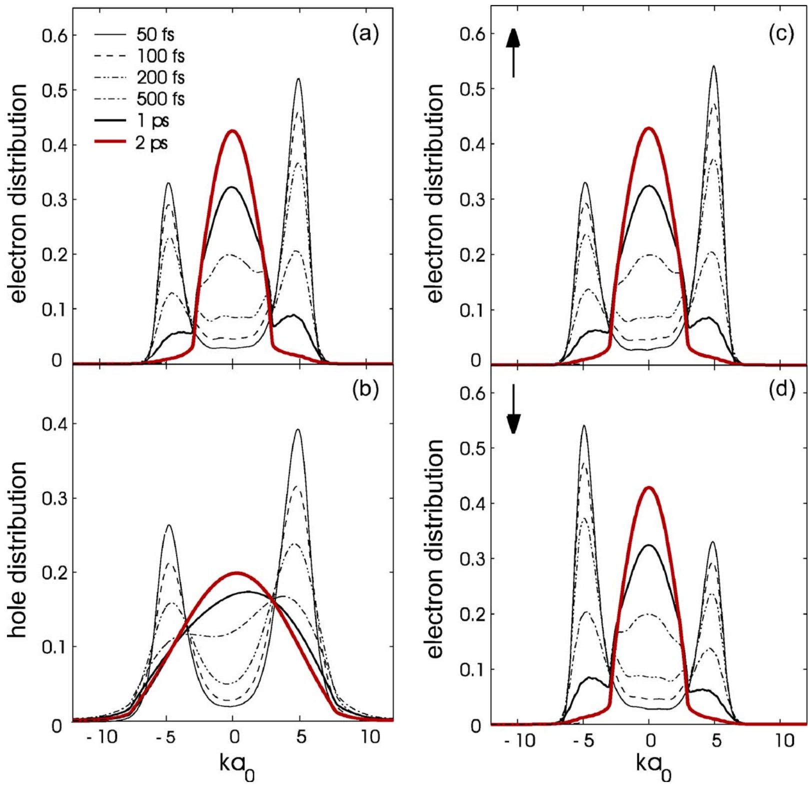

FIG. 2. (Color online) Relaxation dynamics of the photogenerated carriers in k space caused by carrier–LO-phonon and carrier-carrier scattering. (a) and (b) show snapshots of the electron and the hole distributions for the case in which a charge current has been excited with linear parallel polarized ω and 2ω fields. In this case, the distributions do not depend on the spin. (c) and (d) show snapshots of the distributions of the spin-up and spin-down electrons for the case in which a spin current has been excited with linear perpendicular polarized ω and 2ω fields. Both calculations are performed for the same excitation conditions. The incident pulses have a duration of $\tau_L=20$ fs, the amplitudes are chosen as $A_\omega=2A_{2\omega}$, with $A_{2\omega}=128A_0$, where $A_0=E_0/ea_0\approx 4\times 10^3$ V/cm, E_0 is a three-dimensional exciton Rydberg, and a_0 is the Bohr radius of a three-dimensional exciton. The frequency of the 2ω pulse corresponds to $2\hbar\omega=1.62$ eV, the density of the photoinjected carriers is $N=5\times 10^5$ cm^{-1}, and the temperature is $T=50$ K.

tions $\phi_{2\omega}-2\phi_\omega=\pi/2(\pi)$ to obtain a large charge (spin) current.

The ultrafast laser pulses used in our computations have a duration of $\tau_L=20$ fs. The ratio between the amplitudes of the ω and the 2ω fields is denoted by $x=A_\omega/A_{2\omega}$. In most of the following calculations we use $x=2$, and we chose the amplitudes in order to reach a certain density of photoinduced carriers.

Figures 2(a) and 2(b) show the dynamics of the photoexcited electron and hole distributions in k space for the case in which a charge current is excited. The two incident laser pulses have frequencies of $\hbar\omega=0.81$ eV and $2\hbar\omega=1.62$ eV, respectively, and are polarized as shown in Fig. 1(a). The optical excitation generates the carriers with an excess energy of 120 meV above the band gap. Due their smaller mass, about 105 meV of the kinetic energy is given to the electrons whereas that of the holes is only about 15 meV. Since the energy of the LO phonons is $\hbar\omega_{\mathrm{LO}}=36$ meV, the electron relaxation is considerably influenced by the emission of LO phonons. The hole distribution is, however, only weakly affected by the scattering with LO phonons, since LO-phonon emission is not possible due to their small excess energy. Immediately after the excitation, e.g., at $t=50$ fs, the electron and hole distributions are very similar, see Figs. 2(a) and 2(b). Both show maxima around $k=\pm 5/a_0$ and the peaks at positive k are larger than the ones at negative k, i.e., the distributions are not symmetric in k space,[2] which, according to Eq. (15), corresponds to a nonvanishing charge current. If only the 2ω pulse were considered, the initial peaks of the distributions around $k=\pm 5/a_0$ would be symmetric since in this case interband excitations dominate. The interference between the ω and 2ω pulses involves intraband excitations that lead to the asymmetries in the k-space distributions, as is shown in Appendix B. Since the scattering processes exchange momentum among the carriers and with the phonon system, the degree of asymmetry decreases with increasing time. In the limit of long times, the electron and hole distributions both approach quasiequilibrium distributions in their respective bands, see Figs. 2(a) and 2(b). Due to their larger mass, the hole distribution is significantly broader than that of the electrons.

Figures 2(c) and 2(d) show the dynamics of the distributions of the spin-up and the spin-down electrons in k space for the case in which a spin current has been excited. It can be clearly seen that the spin-dependent electron distributions are mirror images of each other, i.e., that the relation $n^e_{\uparrow k}=n^e_{\downarrow -k}$ holds. Since the same relation also holds for the holes (not shown in figure), according to Eq. (15) the charge current vanishes and a pure spin current, see Eq. (16), is generated. The relaxation dynamics of the electron distribution in Fig. 2(c) is very similar to the case in which a charge current has been excited, see Fig. 2(a).

The computed time dependencies of the charge and spin currents corresponding to the situation displayed in Fig. 2 are shown by the thick solid lines in Figs. 3(a) and 3(b). Note that due to their smaller mass, both currents are predominantly due to the electrons. As a result of the relaxation and the concomitant reduction of the asymmetric parts of the k-space distributions, the initially generated currents decrease with time. The decays are nonexponential, however up to about 1 ps they can be approximated by exponential decays with time constants of $\tau\approx 680$ fs for the case of the charge current and $\tau\approx 530$ fs for the case of the spin current. If the carrier-carrier scattering is neglected, see the dashed lines in Figs. 3(a) and 3(b), the dampings of the charge and the spin currents are slower and the carrier–LO-phonon scat-

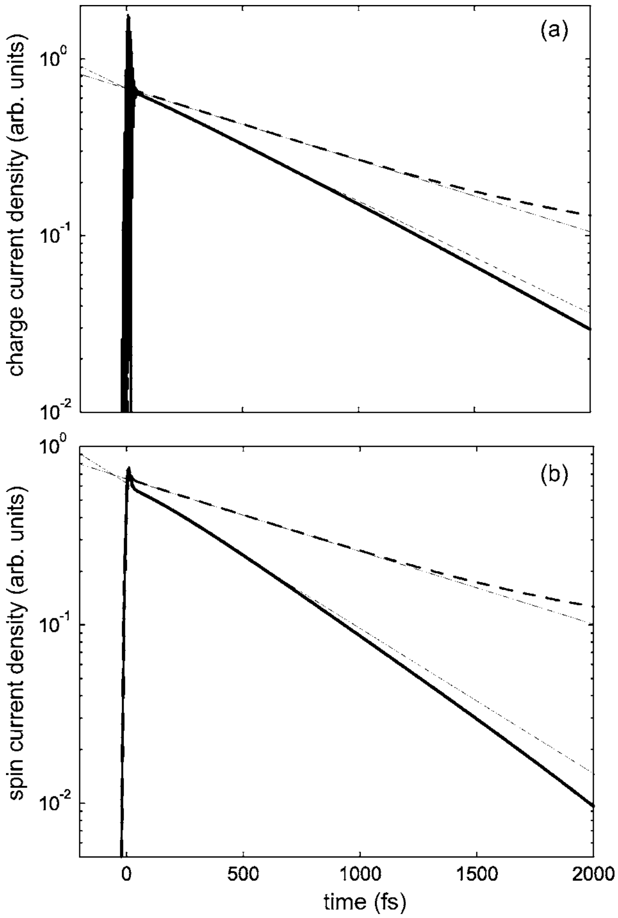

FIG. 3. Time dependence of the charge (a) and the spin (b) current densities. The parameters are the same as in Fig. 2. The thick solid line shows the dynamics including both carrier–LO-phonon and carrier-carrier scattering processes, whereas the dashed lines have been calculated considering only carrier–LO-phonon scattering. The thin solid lines represent exponential decays $\propto \exp(-t/\tau)$ with time constants of $\tau=1050$ and 680 fs in (a) and of $\tau=1050$ and 530 fs in (b), respectively.

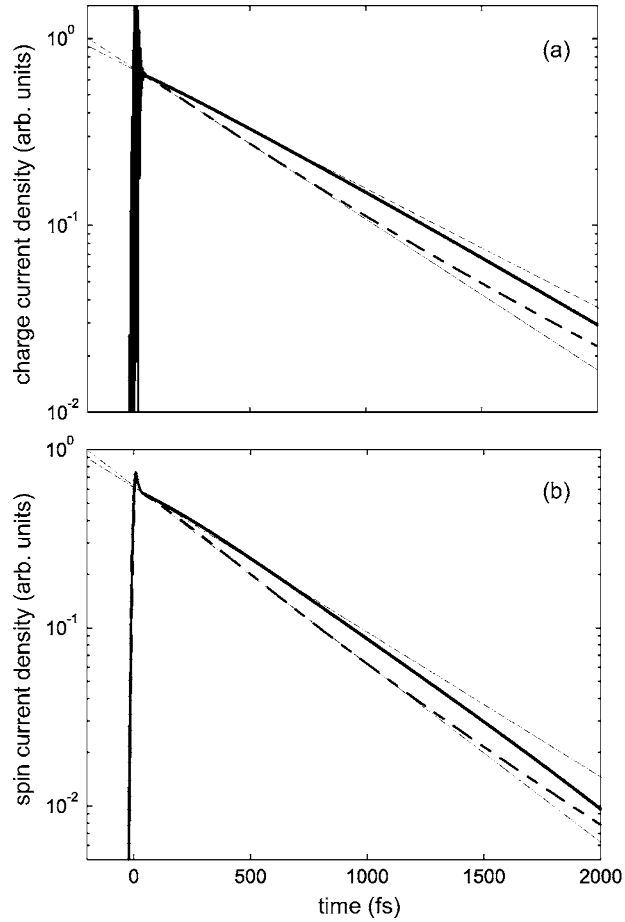

FIG. 4. Time dependence of the charge (a) and the spin (b) current densities including carrier–LO-phonon and carrier-carrier scattering at two temperatures. The thick solid and dashed lines show the dynamics at $T=50$ and 300 K, respectively. The other parameters are the same as in Fig. 2. The thin solid lines represent exponential decays $\propto \exp(-t/\tau)$ with time constants of $\tau=680$ and 540 fs in (a) and of $\tau=570$ and 470 fs in (b), respectively.

tering alone produces an identical decay characterized by a time constant of $\tau \approx 1050$ fs for both currents. Thus for a density of $N=5\times10^5$ cm^{-1}, the carrier-carrier scattering significantly speeds up the relaxation dynamics. This is to be expected, since for the considered excitation conditions the maxima of the photogenerated electron and hole distributions are comparable to 1, see Figs. 2(a) and 2(b), i.e., the photoexcitation is not in the low-intensity limit. Furthermore, as has already been demonstrated in Ref. 16, the carrier-carrier scattering leads to a more rapid decay of the spin current as compared to that of the charge current. Further calculations, in which different scattering processes have artificially been switched off, have shown that the different dampings of the charge and spin currents result from the Coulomb scattering among carriers with opposite spin. This process exchanges momentum between the carriers with opposite spin and is therefore able to symmetrize the k-space distributions of the spin-up and spin-down carriers for a situation corresponding to a spin current as shown in Figs. 2(c) and 2(d). For the case of a charge current, both spins are excited identically and carry the same nonvanishing average momentum, which cannot be reduced by momentum-exchanging carrier-carrier scattering.

The influence of the temperature on the decay of the charge and spin current densities is shown in Figs. 4(a) and 4(b). Increasing the temperature from 50 to 300 K noticeably speeds up the initial decay of both the charge and the spin currents, since at elevated temperatures the population of LO phonons is increased and therefore the carrier–LO-phonon scattering is more rapid. Comparing the approximate decay times of the charge and the spin currents at the two temperatures, one finds that at 50 K the spin current decays about 19% more rapidly than the charge current, whereas at 300 K the decay is enhanced by only about 15%. A reduction of this difference is to be expected since at elevated temperatures the relative importance of the carrier-carrier scattering, which is responsible for the different decay times of the charge and the spin currents, is reduced. Qualitatively similar results regarding the influence of the temperature on the current decay due to carrier–LO-phonon scattering in bulk semiconductors have been reported in Ref. 5.

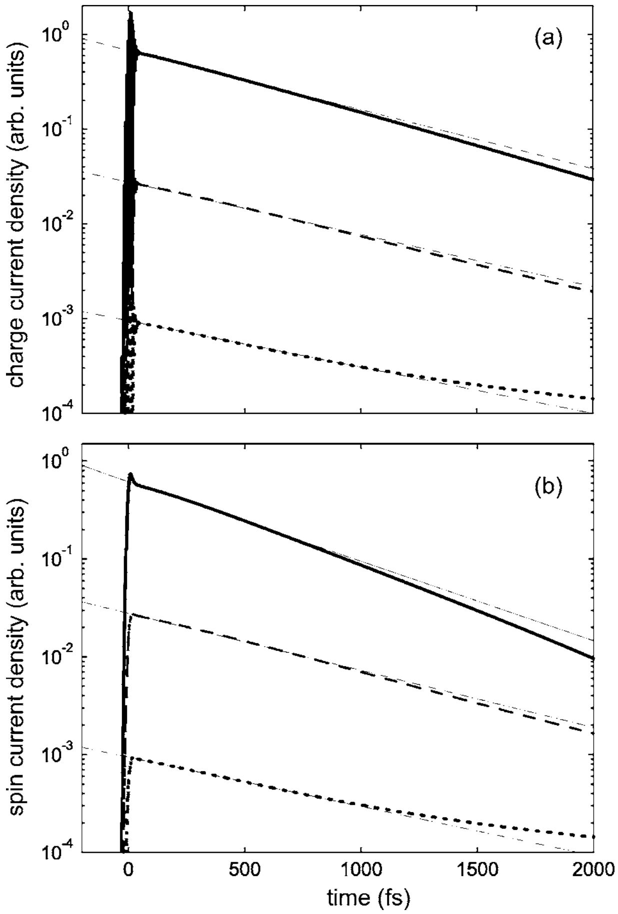

FIG. 5. Time dependence of the charge (a) and the spin (b) current densities including carrier–LO-phonon and carrier-carrier scattering at three densities. The thick solid, dashed, and dotted lines show the dynamics at $N=5\times10^5$ cm^{-1}, 5×10^4 cm^{-1}, and 5×10^3 cm^{-1}, respectively. To generate these carrier densities, field amplitudes of $A_{2\omega}=A_\omega/2=128A_0$, $A_{2\omega}=A_\omega/2=38A_0$, and $A_{2\omega}=A_\omega/2=12A_0$, respectively, are used. The other parameters are the same as in Fig. 2. The thin solid lines represent exponential decays $\propto\exp(-t/\tau)$ with time constants of $\tau=680$, 790, and 860 fs in (a) and of $\tau=530$, 750, and 850 fs in (b), respectively.

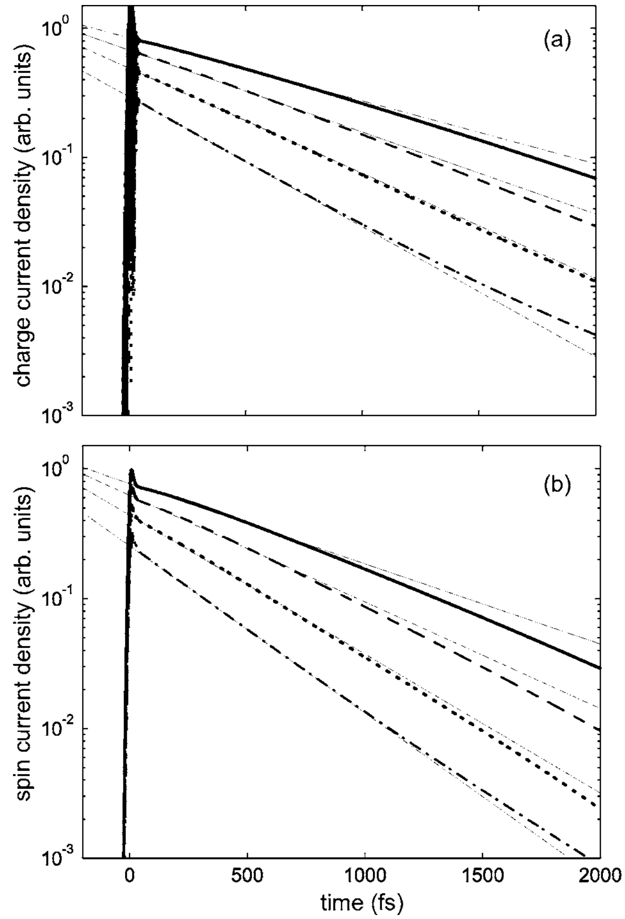

FIG. 6. Time dependence of the charge (a) and the spin (b) current densities including carrier–LO-phonon and carrier-carrier scattering at different excitation frequencies. The thick solid, dashed, dotted, and dashed-dotted lines shows the dynamics at $2\hbar\omega=1.65$, 1.62, 1.59, and 1.56 eV, respectively. The density of the photoinjected carriers is $N=5\times10^5$ cm^{-1} in each case. To generate this carrier density, field amplitudes of $A_{2\omega}=A_\omega/2=140A_0$, $A_{2\omega}=A_\omega/2=128A_0$, $A_{2\omega}=A_\omega/2=115A_0$, and $A_{2\omega}=A_\omega/2=100A_0$, respectively, are used. The other parameters are the same as in Fig. 2. The thin solid lines represent exponential decays $\propto\exp(-t/\tau)$ with time constants of $\tau=870$, 680, 530, and 430 fs in (a) and of $\tau=700$, 530, 400, and 340 fs in (b), respectively.

By varying the amplitudes of the incident light fields, we can analyze how the charge and spin currents decay for different densities of the photoexcited carriers. The initial amplitude of the charge current, see Fig. 5(a), decreases and its decay becomes slower with decreasing density. This is due to the fact that the carrier-carrier scattering becomes less rapid when a smaller density is present. Thus, in the limit of very small densities the decay is governed entirely by carrier–LO-phonon scattering. The dependence of the dynamics of the spin current on the carrier density is displayed in Fig. 5(b). As the charge current, see Fig. 5(a), also the initial amplitude of the spin current decreases and its decay becomes slower with decreasing density. Thus, for very low densities, the decay of both currents is mainly governed by the carrier–LO-phonon scattering since the carrier-carrier scattering becomes very slow. Consequently, the relative difference of the decay times of the charge and the spin currents gets smaller with decreasing carrier density.

In the low-intensity limit, the carrier density and the charge and spin currents can be described by the perturbative approach presented in Appendix B. To lowest order in the light fields, the density is proportional to the product of two field amplitudes, i.e., $N\propto A_{\nu'}A_{\nu''}$, whereas the currents are at least of third order in the field, i.e., $J,S\propto A_{\nu'}A_{\nu''}A_{\nu'''}$, where ν', ν'', and ν''' are either ω or 2ω. If A_ω and $A_{2\omega}$ are comparable, the resonant 2ω interband transitions predominantly excite the density in second order and therefore $N\propto A_{2\omega}^2$ holds. The currents are generated by interacting with the 2ω field once and the ω field twice, i.e., $J,S\propto A_\omega^2 A_{2\omega}$, since this excitation scheme is able to resonantly create asymmetric third-order populations in k space. If the excitation is in the low-intensity limit and the ratio between A_ω and $A_{2\omega}$ is kept constant, a change of the carrier density N by a factor η requires us to change the field amplitudes by $\sqrt{\eta}$. The cur-

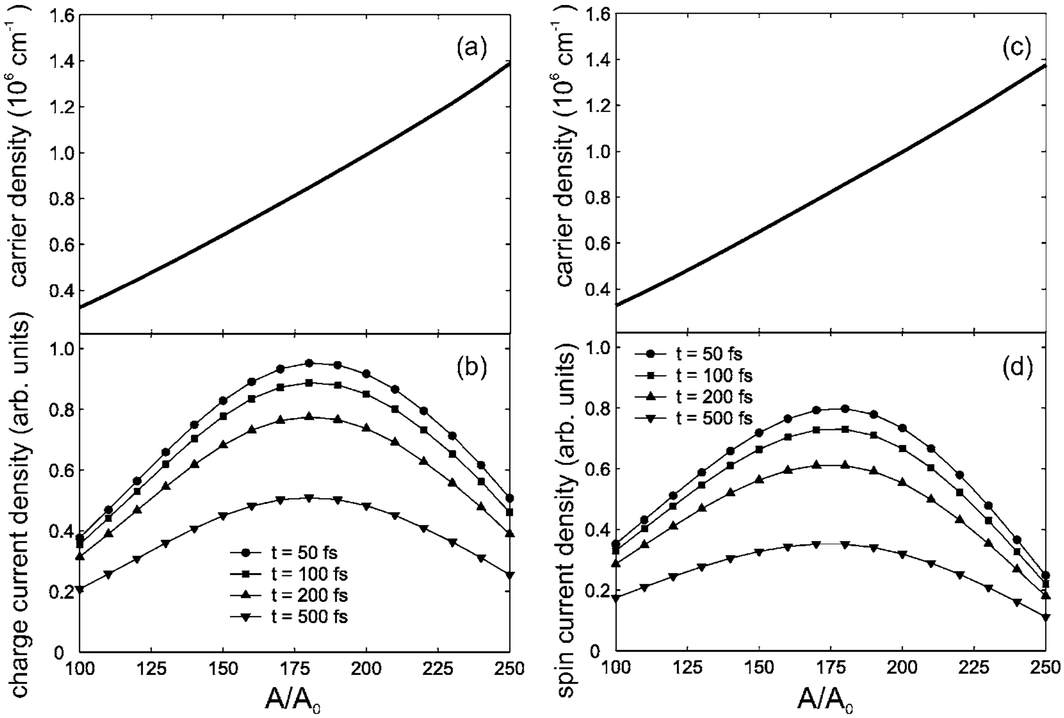

FIG. 7. Dependence of (a) the carrier density and (b) the charge current density at $t=50$, 100, 200, and 500 fs on the amplitude A of the incident pulses including carrier–LO-phonon and carrier-carrier scattering. $A=A_{2\omega}=A_{\omega}/2$ is measured in units of $A_0=E_0/ea_0\approx 4\times 10^3$ V/cm, where E_0 is a three-dimensional exciton Rydberg. The other parameters are the same as in Fig. 2. (c) and (d) show the same as (a) and (b) for the excitation of a spin current instead of a charge current. (a) and (b) correspond to Figs. 3(a) and 3(b) of Ref. 16.

rents are therefore proportional to $\eta^{1.5}$. This analysis explains why the initial amplitudes of the currents shown in Figs. 5(a) and 5(b) change by a factor of approximately 30 when the carrier density changes only by a factor of 10.

Figure 6(a) shows the time-dependent charge currents calculated for different excitation frequencies of the laser pulses. In order to ensure that the carrier density is constant ($N=5\times 10^5$ cm^{-1}) when varying the frequencies, the amplitudes of light fields were adjusted appropriately. With decreasing excitation frequency, the initial magnitude of the current decreases since the kinetic energy and thus the momentum of the photogenerated carriers decreases. Additionally, the initial decay of the current becomes more rapid with decreasing excitation frequency. This behavior is due to the strong dependence of the LO-phonon emission rate on the carrier energy, which in our model calculations is significantly influenced by the one-dimensional density of states. It has been shown[36,37] that the one-dimensional LO-phonon emission rate has a singularity when the kinetic energy of the carriers is equal to the energy of the LO phonons and becomes smaller at higher energies. When exciting with $2\hbar\omega=1.56$ eV, the initially rapid current decay slows down for longer times, see Fig. 6(a). The reason for the transient slowing down of the decay is that the electrons are created with an initial kinetic energy of about 52 meV, which means that they can emit only a single LO phonon. Thus, at long times the initially rapid relaxation due to LO-phonon emission is suppressed and the subsequent decay is dominated by the carrier-carrier scattering. The dependence of the spin current on the excitation frequency of laser fields is shown in Fig. 6(b). As for the charge current, see Fig. 6(a), also the initial magnitude of the spin current becomes smaller and its initial decay gets more rapid with decreasing excitation frequency.

Figure 7(a) shows how the injected carrier density depends on the amplitudes $A=A_{2\omega}=A_{\omega}/2$ of the fields, when their ratio is kept equal. In the considered regime, the density increases approximately linearly with A. The charge current, however, depends on A in a strongly nonlinear fashion, see Fig. 7(b). It has a maximum at $A\approx 180A_0$ and decreases for smaller and larger amplitudes. In the low-intensity limit, the k-space carrier distributions increase with A without significant distortion. Therefore, in this regime both the total density and the charge current become larger with increasing A. At a certain excitation level, however, the peaks of the generated distributions at $k=\pm 5/a_0$, see Fig. 2, become comparable to 1 and further excitation is suppressed by the Pauli exclusion principle. Additionally, the intraband acceleration broadens the distributions over larger regions in k space. As a result, the photogenerated carrier distributions become more symmetric in k space and subsequently the charge current decreases when the field amplitude is increased further. The results shown in Figs. 7(c) and 7(d) for the excitation of a spin current are very similar to the ones obtained for the charge current, see Figs. 7(a) and 7(b). In particular, the largest spin current is obtained for about the same field amplitudes, which also maximize the charge current.

Figures 8(a) and 8(b) show how the carrier density and the charge current density depend on the ratio of the amplitudes of the two incident pulses $x=A_{\omega}/A_{2\omega}$ for a fixed amplitude of the 2ω field, $A_{2\omega}=128A_0$. Note that all previous

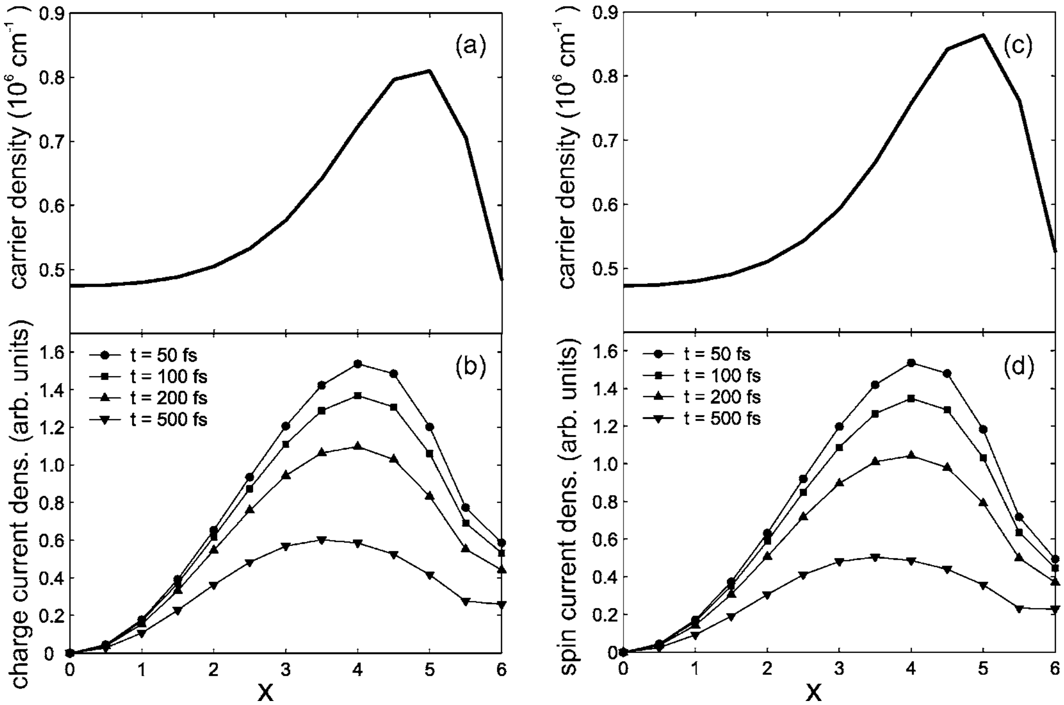

FIG. 8. Dependence of (a) the carrier density and (b) the charge current density at $t=50$, 100, 200, and 500 fs on the amplitude ratio $x=A_\omega/A_{2\omega}$ for $A_{2\omega}=128A_0$ including carrier–LO-phonon and carrier-carrier scattering. The other parameters are the same as in Fig. 2. (c) and (d) show the same as (a) and (b) for the excitation of a spin current instead of a charge current. (a) and (b) correspond to Figs. 3(c) and 3(d) of Ref. 16.

results were obtained for $x=2$. At $x=0$, only the 2ω field is present and therefore the photoexcited carrier distributions are symmetric in k space. Consequently, in this case the current vanishes. For the generation of a finite current, a finite x is required, i.e., the amplitude of the ω field must not vanish. Both fields are necessary since the interference of interband and intraband excitations is needed for the photoexcitation of nonsymmetric k-space carrier distributions. With increasing x, the current starts to rise significantly, whereas the carrier density increases only slightly, see Figs. 8(a) and 8(b). This is due to the fact that a rather weak ω field predominantly redistributes the carriers in k space by introducing asymmetries without enhancing the density, as is shown by the perturbative analysis presented in Appendix B. At a certain A_ω, however, due to the above-mentioned Pauli-blocking and k-space averaging effects, a further increase of the current is not possible. Therefore, for a fixed $A_{2\omega}$ there exists an optimal A_ω that leads to a maximal asymmetry of the photogenerated distributions and thus to a maximal current. For $A_{2\omega}=128A_0$, the largest current is obtained for $A_\omega \approx 512A_0$, i.e., for $x\approx 4$. For amplitudes $A_{2\omega}$ smaller than $128A_0$, the optimal ratio x is larger than 4. This can be understood since in the perturbative regime the current is linear in the 2ω field but of second order in the ω field. Thus the optimal current requires a very large x since the second-order excitations induced by the ω field have to be comparable to the linear ones generated by the 2ω field. Figures 8(c) and 8(d) show that when switching the light polarizations from charge to spin current excitation, the dependencies of the carrier density and the current density on the ratio x remain basically unchanged.

B. Quantum-kinetic calculations of the charge and spin current dynamics

In this section, the transients of the charge and spin current densities are investigated on the level of a non-Markovian quantum-kinetic theory for the carrier-carrier and the carrier–LO-phonon interactions. Here, we neglect the exchange terms of the Coulomb quantum kinetics. First of all, it has been shown[30,38,39] that the contributions of these terms are not very important for the analysis of ultrafast scattering processes. Secondly, this approximation keeps the numerical requirements within reasonable limits, particularly in the present case in which we cannot use the rotating-wave approximation for the analysis of the charge and spin currents. The Coulomb potential is treated in the random-phase approximation. It is well known that this approximation leads to a long-wavelength divergence within the two-time quantum-kinetic formalism. However, as shown in Ref. 40, these divergencies cancel out within the generalized Kadanoff-Baym ansatz, which is used here to replace the two-time functions by single-time functions. The generalized Kadanoff-Baym ansatz is also justified for the treatment of the LO-phonon quantum kinetics as long as the electron-phonon interaction is not in the strong-coupling regime.[41]

The temporal dynamics of the charge current is shown in Fig. 9(a) for different photoexcited carrier densities. We see that the non-Markovian quantum kinetics (QK), thick solid lines, and the Markov approximation (MA), thin solid lines, yield basically the same density-dependent decay of the charge current. The comparison with the results obtained on the second Born-Markov level (2BMA), thick dotted lines, shows that without exchange terms the decay time of the

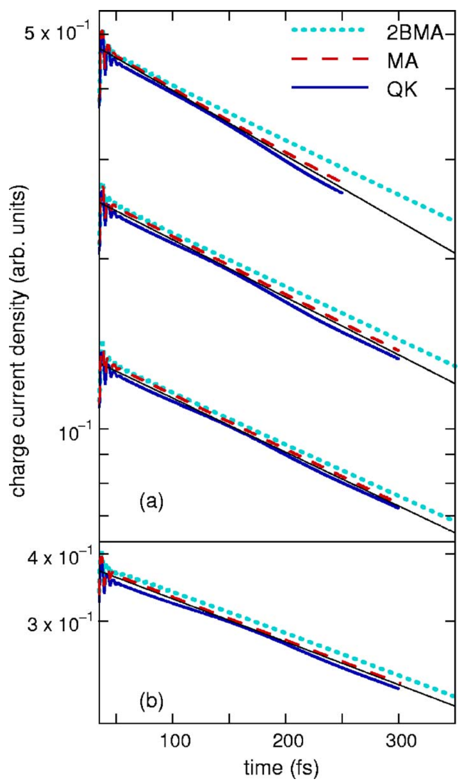

FIG. 9. (Color online) (a) Time dependence of the charge current density including carrier–LO-phonon and carrier-carrier scattering for different approximations, i.e., on the second Born-Markov level (2BMA), the quantum-kinetic approach (QK), and with the Markov approximation neglecting the exchange terms (MA). The calculations have been performed for carrier densities of $N_1=5\times10^5$ cm^{-1}, $N_2=3\times10^5$ cm^{-1}, and $N_3=2\times10^5$ cm^{-1} (from top to bottom) at $T=300$ K and with $2\hbar\omega=1.59$ eV. To generate these carrier densities, field amplitudes of $A_{2\omega}=A_\omega/2=115A_0$, $A_{2\omega}=A_\omega/2=87A_0$, and $A_{2\omega}=A_\omega/2=70A_0$, respectively, are used. The thin solid lines represent exponential decays $\propto\exp(-t/\tau)$ with $\tau_{N_1}=376$ fs, $\tau_{N_2}=425$ fs, and $\tau_{N_3}=455$ fs for the QK calculations. The decay times of the charge current density for the 2BMA calculations are $\tau_{N_1}=445$ fs, $\tau_{N_2}=460$ fs, and $\tau_{N_3}=475$ fs (not shown by lines). (b) The charge current density for $2\hbar\omega=1.62$ eV and a density of $N=N_2$ that is generated using $A_{2\omega}=A_\omega/2=96A_0$. The other parameters are the same as in (a). The corresponding decay times are $\tau=570$ fs for the QK calculations (see the thin solid line) and $\tau=585$ fs 2BMA (not shown by a line), respectively.

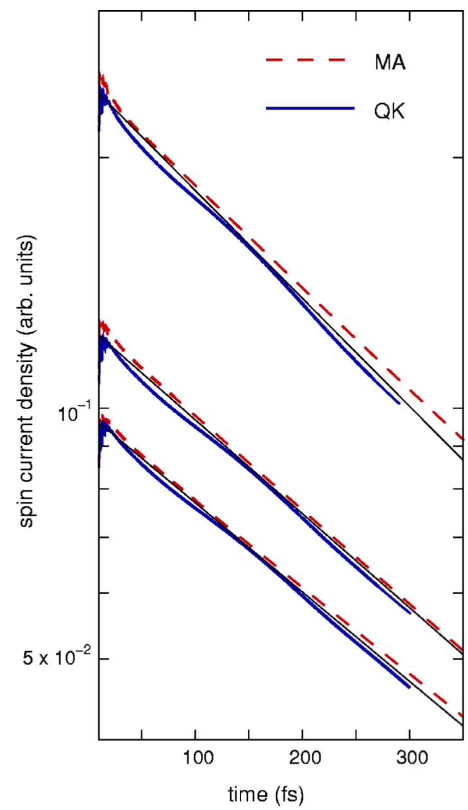

FIG. 10. (Color online) Time dependence of the spin current density including carrier–LO-phonon and carrier-carrier scattering for different approximations, i.e., the quantum-kinetic approach (QK) and with the Markov approximation neglecting the exchange terms (MA). The calculations have been performed for carrier densities of $N_2=3\times10^5$ cm^{-1}, $N_3=2\times10^5$ cm^{-1}, and $N_4=1.2\times10^5$ cm^{-1} (from top to bottom) at $T=300$ K and with $2\hbar\omega=1.59$ eV. To generate these carrier densities, field amplitudes of $A_{2\omega}=A_\omega/2=87A_0$, $A_{2\omega}=A_\omega/2=70A_0$, and $A_{2\omega}=A_\omega/2=54A_0$, respectively, are used. The thin solid lines represent exponential decays $\propto\exp(-t/\tau)$ with $\tau_{N_2}=335$ fs, $\tau_{N_3}=385$ fs, and $\tau_{N_4}=405$ fs.

charge current is underestimated by less than 20% for a carrier density of $N_1=5\times10^5$ cm^{-1}. At smaller carrier densities, the contribution of the exchange terms decreases. As on the second Born-Markov level, also within the quantum-kinetic approach, the decay of the charge current becomes more rapid with increasing carrier density and temperature and when we decrease the frequencies of the incident laser pulses (not shown in figure). Besides a small change in the overall magnitude, an interesting feature of the quantum-kinetic results is the weak oscillations that are visible in the decaying charge current transients. When varying the carrier density from 2×10^5 to 5×10^5 cm^{-1}, the period of the oscillations remains almost unchanged and is about 170 fs.

The oscillations with the carrier-density-independent period of about 170 fs appear also in the spin current, see Fig. 10. Besides this characteristic feature, we find that also within the quantum-kinetic approach, (i) the decay of the spin current becomes more rapid with increasing carrier density ($\tau_{N_2}=335$ fs and $\tau_{N_3}=385$ fs, see the solid lines with $N_2=3\times10^5$ cm^{-1} and $N_3=2\times10^5$ cm^{-1} in Fig. 10), and (ii) the spin current decays faster in comparison to the charge current ($\tau_{N_2}=425$ fs and $\tau_{N_3}=455$ fs, see the solid lines with $N_2=3\times10^5$ cm^{-1} and $N_3=2\times10^5$ cm^{-1} in Fig. 9). Thus, we find that apart from additional oscillations, the time dependencies of the charge and spin current densities obtained from the quantum-kinetic calculations are very similar to the results obtained on the second Born-Markov level, which have been presented in Sec. IV A.

In order to understand the origin of the oscillations in the current transients, the charge current $J=J_e+J_h$ and its electron and hole components J_e and J_h (multiplied by 7) are presented separately in Fig. 11(a) for different approximations made within the quantum-kinetic calculations. For all considered cases, the current component of the electrons J_e decays monotonously and close to exponential as a function of time without any visible superimposed oscillations. If only

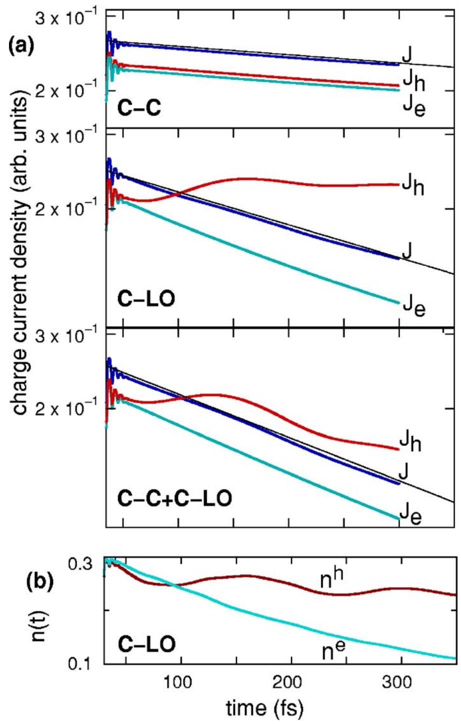

FIG. 11. (Color online) (a) Time dependence of the charge current density $J=J_e+J_h$ and its electron J_e and hole J_h components computed within the quantum-kinetic approach for different approximations, i.e., with only carrier-carrier scattering (C-C), with only carrier–LO-phonon scattering (C-LO), and with carrier-carrier and carrier–LO-phonon scattering (C-C+C-LO), at $T=300$ K and with $2\hbar\omega=1.59$ eV. For better visibility, the hole component J_h has been multiplied by a factor of 7. The thin solid lines represent exponential decays $\propto\exp(-t/\tau)$ with time constants of 2200, 560, and 420 fs (from top to bottom). In these calculations, the carrier density is $N_2=3\times10^5$ cm^{-1}. To generate this carrier density, field amplitudes of $A_{2\omega}=A_\omega/2=87A_0$ are used. (b) The electron and hole populations, i.e., n^e and n^h, at the energetic position of the initial photoexcitation with only carrier–LO-phonon scattering (C-LO) considered. The parameters are the same as in (a).

the carrier-carrier scattering (C-C) is considered, J, J_e, and J_h decay identically with a rather slow time constant $\tau=2200$ fs and no oscillations are present. However, if carrier–LO-phonon scattering is considered (C-LO and C-C+C-LO), the hole contribution to the current J_h shows oscillations with a very pronounced amplitude and a period of about 170 fs. This oscillation is also visible in the time-dependent hole population $n_h(t)$ at the energetic position of the initial photoexcitation displayed in Fig. 11(b). Therefore, we have identified that the coupling of the holes to the LO phonons is the dominant source of the oscillations. Due to the large mass of the heavy holes ($m_h\approx7m_e$), the contribution of the oscillations present in J_h to the total current J is rather weak. As a result, the total current density J is predominantly decaying and shows only weak additional modulations with the period of 170 fs. Figure 11(a) furthermore shows that neglecting the carrier-carrier scattering (C-LO) significantly reduces the amplitude of the oscillations in the current J. This is due to the fact that in the presence of carrier-carrier scattering, which broadens the distributions in

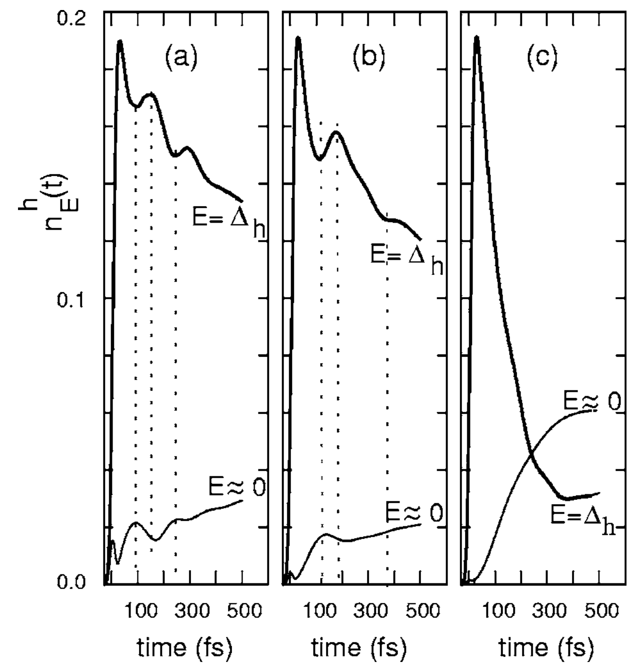

FIG. 12. Time dependence of the hole population $n_E^h(t)$ computed within the quantum-kinetic approach considering only carrier–LO-phonon scattering at two energies $E=\Delta_h$ (thick line) and $E\approx0$ meV (thin line). The considered excess energies $\Delta=2\hbar\omega-E_{\mathrm{gap}}$ are (a) $\Delta=90$ meV, (b) $\Delta=150$ meV, and (c) $\Delta=260$ meV at $T=300$ K. This results in excess hole energies of $\Delta_h=11.5$ meV (a), $\Delta_h=19.2$ meV (b), and $\Delta_h=33.2$ meV (c). In these single-pulse calculations, we set $A_\omega=0$ and $A_{2\omega}=40A_0$. This results in carrier densities of 1.2×10^5 cm^{-1} (a), 0.95×10^5 cm^{-1} (b), and 0.8×10^5 cm^{-1} (c), respectively.

k space, the carrier–LO-phonon scattering is enhanced.

To gain a more detailed understanding of the quantum-kinetic oscillations, we have computed results considering only the carrier–LO-phonon scattering and just the 2ω pulse. In these calculations, the Coulomb scattering is replaced by a phenomenological dephasing time of $T_2=250$ fs for the interband polarization. Figure 12 shows the time evolution of the hole population $n_E^h(t)$ at two energetic positions, namely at the position $E=\Delta_h$ where the holes are optically created and at the band edge $E\approx0$ meV. Here, $\Delta_h=(m_r/m_h)\Delta$ is the hole excess energy, $\Delta=2\hbar\omega-E_{\mathrm{gap}}$ is the total excess energy, and m_r is the reduced mass. For an excess energy of $\Delta=90$ meV, see Fig. 12(a), the hole is excited with a kinetic energy of $\Delta_h\approx11.5$ meV. Therefore, no real LO-phonon emission processes are possible for the holes. The well-resolved oscillations have a period of 160 fs. The dotted lines in Fig. 12 allow us to see more clearly that the hole populations at $E=\Delta_h$ and at $E\approx0$ meV (band edge) oscillate out of phase, i.e., a minimum at Δ_h coincides with a maximum at the band edge, and vice versa.

These quantum-kinetic oscillations are a consequence of virtual scattering processes. The holes excited at $E=\Delta_h$ try to relax via the emission of an LO phonon to the band gap at $E=0$. Since Δ_h is smaller than the LO-phonon energy $\hbar\omega_{\mathrm{LO}}$, this relaxation process does not fulfill energy conservation. As a consequence, this virtual process cannot be completed and the hole populations at $E=\Delta_h$ and $E=0$ oscillate temporally out of phase. The oscillation period is determined by the energy mismatch, i.e., $\Delta_h - \hbar\omega_{\mathrm{LO}}$, and approximately given by

$$\Delta t \approx \frac{2\pi\hbar}{\hbar\omega_{\mathrm{LO}} - \Delta_h}. \tag{24}$$

For a detuning of $\Delta = 90$ meV, i.e., $\Delta_h = 11.5$ meV, we get $\Delta t \approx 165$ fs, which coincides with the period found with the quantum-kinetic calculations, see Fig. 12(a). For an excitation with an excess energy of $\Delta = 150$ meV, i.e., $\Delta_h = 19.2$ meV, we have computed, see Fig. 12(b), a slower oscillation period of about 250 fs, which is in agreement with the period determined by Eq. (24) of 246 fs. For the largest considered detuning $\Delta = 260$ meV, where $\Delta_h = 33.2$ meV approaches the LO-phonon energy of 36 meV, we find during the first 500 fs a decrease (an increase) of the hole population at Δ_h (0), see Fig. 12(c). Thus the oscillation period has to be longer than 1000 fs, which is again compatible with the oscillation period of ≈ 1500 fs obtained from Eq. (24). At this larger detuning, irreversible relaxation due to real scattering processes starts to become relevant.

V. CONCLUSIONS

A microscopic many-body theory that is capable of describing the coherent optical injection of charge and spin currents and their temporal evolution has been presented. The approach is based on the semiconductor Bloch equations and nonperturbatively includes light-field-induced intraband and interband excitations. Besides excitonic Coulomb effects in the Hartree-Fock approximation, also carrier–LO-phonon and carrier-carrier scattering processes are treated.

The theory has been used to evaluate numerically the dynamics of the carrier distributions and of the charge and spin currents for a one-dimensional model system. When evaluating the scattering processes on the second Born-Markov level, we find that with increasing temperature the carrier–LO-phonon scattering rates increase and subsequently the decay of the charge and spin currents becomes more rapid. The LO-phonon emission rate becomes smaller if the kinetic energy of the carriers increases and consequently the decay times of the currents get longer. With increasing carrier density, the carrier-carrier scattering becomes more rapid and thus the currents decay faster. We have also investigated how the currents behave when varying the field amplitudes and the ratio between the amplitudes of the ω and the 2ω fields. For both cases, we find nontrivial field parameters that maximize the currents since for strong fields (i) the density of excited carriers is limited by phase-space filling effects and (ii) the intraband acceleration significantly broadens the carrier distributions in k space.

Our analysis demonstrates that at low carrier densities, where carrier–LO-phonon scattering dominates, the charge and spin currents decay on the same time scale, whereas at higher densities, due to carrier-carrier scattering processes between particles with different spin, the decay of the spin current is faster than that of the charge current.[16] The influences of the temperature, the carrier density, the excitation frequency, and the intensity of the pulses are very similar for both currents. Due to the inefficient scattering in one dimension, the obtained decay times for the one-dimensional model system are rather long. When evaluating our theory for two-dimensional systems, we find that typical decay times are shorter and in the range of 100–200 fs.[16]

When evaluating the scattering contributions at the quantum-kinetic level, we confirm the basic decay dynamics of our second Born-Markov theory. However, our results predict that memory effects can lead to additional oscillatory signatures in the decaying current transients. Our analysis attributes the quantum-kinetic oscillations to the virtual emission of LO phonon, when the kinetic energy of the photoexcited holes is smaller than the energy of the LO phonons.

ACKNOWLEDGMENTS

This work is supported by the Deutsche Forschungsgemeinschaft (DFG), by the German Ministry for Education and Research (BMBF), and by the Center for Optodynamics, Philipps University, Marburg, Germany. We thank the John von Neumann Institut für Computing (NIC), Forschungszentrum Jülich, Germany, for grants for extended CPU time on their supercomputer systems. T.M. thanks the DFG for support (ME 1916/1).

APPENDIX A: COLLISION CONTRIBUTIONS

The collision terms appearing in Eqs. (8)–(10) originate from the carrier-phonon and the carrier-carrier interaction. We therefore write

$$\left.\frac{d}{dt}x_{\sigma\mathbf{k}}\right|_{\mathrm{coll}} = \left.\frac{d}{dt}x_{\sigma\mathbf{k}}\right|_{c\text{-ph}} + \left.\frac{d}{dt}x_{\sigma\mathbf{k}}\right|_{c\text{-}c}, \tag{A1}$$

with $x = n^e$, n^h, and p.

1. Collision contributions in the second Born-Markov approximation

Both processes are treated up to second order in the respective interaction and the Markov approximation is applied.

a. Carrier-phonon scattering

Considering the carrier-phonon interaction on the second Born-Markov level results in the following terms:[25,26]

$$\begin{aligned}\left.\frac{d}{dt}n^{\mu}_{\sigma\mathbf{k}}\right|_{c\text{-ph}} = {} & \frac{2\pi}{\hbar}\sum_{\mathbf{q}} g^2_{\mathbf{q}}\delta(\varepsilon^{\mu}_{\mathbf{k+q}} - \varepsilon^{\mu}_{\mathbf{k}} - \hbar\omega_{\mathbf{q}})[n^{\mu}_{\sigma\mathbf{k+q}}(1 - n^{\mu}_{\sigma\mathbf{k}}) \\ & \times(N_{\mathbf{q}} + 1) - n^{\mu}_{\sigma\mathbf{k}}(1 - n^{\mu}_{\sigma\mathbf{k+q}})N_{\mathbf{q}}] \\ & - \frac{2\pi}{\hbar}\sum_{\mathbf{q}} g^2_{\mathbf{q}}\delta(\varepsilon^{\mu}_{\mathbf{k+q}} - \varepsilon^{\mu}_{\mathbf{k}} + \hbar\omega_{\mathbf{q}}) \\ & \times[n^{\mu}_{\sigma\mathbf{k}}(1 - n^{\mu}_{\sigma\mathbf{k+q}})(N_{\mathbf{q}} + 1) - n^{\mu}_{\sigma\mathbf{k+q}}(1 - n^{\mu}_{\sigma\mathbf{k}})N_{\mathbf{q}}] \\ & - \frac{1}{\hbar}\sum_{\mathbf{q}} g^2_{\mathbf{q}}\{D(\varepsilon^{\bar{\mu}}_{\mathbf{k}} - \varepsilon^{\bar{\mu}}_{\mathbf{k+q}} - \hbar\omega_{\mathbf{q}})p^{*}_{\mathbf{k+q}}p_{\mathbf{k}} + \mathrm{c.c.}\} \\ & + \frac{1}{\hbar}\sum_{\mathbf{q}} g^2_{\mathbf{q}}\{D(\varepsilon^{\bar{\mu}}_{k} - \varepsilon^{\bar{\mu}}_{k+q} + \hbar\omega_{\mathbf{q}})p^{*}_{\mathbf{k+q}}p_{\mathbf{k}} + \mathrm{c.c.}\},\end{aligned} \tag{A2}$$

$$\left.\frac{d}{dt}p_{\sigma\mathbf{k}}\right|_{c\text{-ph}} = \frac{1}{\hbar}\sum_{\mu\mathbf{q}} g_{\mathbf{q}}^2\{D(\varepsilon^{\mu}_{\mathbf{k+q}} - \varepsilon^{\mu}_{\mathbf{k}} - \hbar\omega_{\mathbf{q}})(N_{\mathbf{q}} + 1 - n^{\mu}_{\sigma\mathbf{k}}) + D(\varepsilon^{\mu}_{\mathbf{k+q}} - \varepsilon^{\mu}_{\mathbf{k}} + \hbar\omega_{\mathbf{q}})(N_{\mathbf{q}} + n^{\mu}_{\sigma\mathbf{k}})\}p_{\mathbf{k+q}} - \frac{1}{\hbar}\sum_{\mu\mathbf{q}} g_{\mathbf{q}}^2\{D(\varepsilon^{\mu}_{\mathbf{k}} - \varepsilon^{\mu}_{\mathbf{k+q}} - \hbar\omega_{\mathbf{q}}) \times (N_{\mathbf{q}} + 1 - n^{\mu}_{\sigma\mathbf{k+q}}) + D(\varepsilon^{\mu}_{\mathbf{k}} - \varepsilon^{\mu}_{\mathbf{k+q}} + \hbar\omega_{\mathbf{q}}) \times (N_{\mathbf{q}} + n^{\mu}_{\sigma\mathbf{k+q}})\}p_{\mathbf{k}}, \tag{A3}$$

where $D(\varepsilon)=iP(1/\varepsilon)+\pi\delta(\varepsilon)$, $\bar{\mu}=h(e)$ for $\mu=e(h)$, and $N_{\mathbf{q}}=[\exp(\hbar\omega_{\mathbf{q}}/k_BT)-1]^{-1}$ is the Bose-Einstein distribution describing a thermal phonon population.

b. Carrier-carrier scattering

On the second Born-Markov level, the Coulomb collision terms are described by[25–29]

$$\begin{aligned}\left.\frac{d}{dt}n^{\mu}_{\sigma\mathbf{k}}\right|_{c\text{-}c} = {}& \frac{2\pi}{\hbar}\sum_{\sigma'\mathbf{k}'\mathbf{q}} W_{\mathbf{q}}(W_{\mathbf{q}} - W_{\mathbf{k}-\mathbf{k}'}\delta_{\sigma\sigma'})\delta(\varepsilon^{\mu}_{\mathbf{k+q}} + \varepsilon^{\mu}_{\mathbf{k}'} - \varepsilon^{\mu}_{\mathbf{k}'+\mathbf{q}} - \varepsilon^{\mu}_{\mathbf{k}})\{n^{\mu}_{\sigma\mathbf{k+q}}n^{\mu}_{\sigma'\mathbf{k}'}(1 - n^{\mu}_{\sigma'\mathbf{k}'+\mathbf{q}})(1 - n^{\mu}_{\sigma\mathbf{k}})\\
&- (1 - n^{\mu}_{\sigma\mathbf{k+q}})(1 - n^{\mu}_{\sigma'\mathbf{k}'})n^{\mu}_{\sigma'\mathbf{k}'+\mathbf{q}}n^{\mu}_{\sigma\mathbf{k}}\} + \frac{2\pi}{\hbar}\sum_{\sigma'\mathbf{k}'\mathbf{q}} W^2_{\mathbf{q}}\delta(\varepsilon^{\mu}_{\mathbf{k+q}} + \varepsilon^{\bar{\mu}}_{\mathbf{k}'+\mathbf{q}} - \varepsilon^{\bar{\mu}}_{\mathbf{k}'} - \varepsilon^{\mu}_{\mathbf{k}})\\
&\times\{n^{\mu}_{\sigma\mathbf{k+q}}n^{\bar{\mu}}_{\sigma'\mathbf{k}'+\mathbf{q}}(1 - n^{\bar{\mu}}_{\sigma'\mathbf{k}'})(1 - n^{\mu}_{\sigma\mathbf{k}}) - (1 - n^{\mu}_{\sigma\mathbf{k+q}})(1 - n^{\bar{\mu}}_{\sigma'\mathbf{k}'+\mathbf{q}})n^{\bar{\mu}}_{\sigma'\mathbf{k}'}n^{\mu}_{\sigma\mathbf{k}}\}\\
&+ \frac{1}{\hbar}\sum_{\sigma'\mathbf{k}'\mathbf{q}} W^2_{\mathbf{q}}\{D(\varepsilon^{\mu}_{\mathbf{k+q}} + \varepsilon^{\bar{\mu}}_{\mathbf{k}'+\mathbf{q}} - \varepsilon^{\bar{\mu}}_{\mathbf{k}'} - \varepsilon^{\mu}_{\mathbf{k}})(n^{\mu}_{\sigma\mathbf{k}} - n^{\mu}_{\sigma\mathbf{k+q}})p^{*}_{\sigma'\mathbf{k}'}p_{\sigma'\mathbf{k}'+\mathbf{q}} + \text{c.c.}\}\\
&+ \frac{1}{\hbar}\sum_{\sigma'\mathbf{k}'\mathbf{q}} W^2_{\mathbf{q}}\{D(\varepsilon^{\bar{\mu}}_{\mathbf{k}} + \varepsilon^{\mu}_{\mathbf{k}'} - \varepsilon^{\mu}_{\mathbf{k}'+\mathbf{q}} - \varepsilon^{\bar{\mu}}_{\mathbf{k+q}})(n^{\mu}_{\sigma'\mathbf{k}'+\mathbf{q}} - n^{\mu}_{\sigma'\mathbf{k}'})p^{*}_{\sigma\mathbf{k+q}}p_{\sigma\mathbf{k}} + \text{c.c.}\}\\
&+ \frac{1}{\hbar}\sum_{\sigma'\mathbf{k}'\mathbf{q}} W_{\mathbf{q}}(W_{\mathbf{q}} - W_{\mathbf{k}-\mathbf{k}'}\delta_{\sigma\sigma'})\{D(\varepsilon^{\mu}_{\mathbf{k+q}} + \varepsilon^{\mu}_{\mathbf{k}'} - \varepsilon^{\mu}_{\mathbf{k}'+\mathbf{q}} - \varepsilon^{\mu}_{\mathbf{k}})(n^{\mu}_{\sigma\mathbf{k}} - n^{\mu}_{\sigma\mathbf{k+q}})p^{*}_{\sigma'\mathbf{k}'+\mathbf{q}}p_{\sigma'\mathbf{k}'} + \text{c.c.}\}\\
&+ \frac{1}{\hbar}\sum_{\sigma'\mathbf{k}'\mathbf{q}} W_{\mathbf{q}}(W_{\mathbf{q}} - W_{\mathbf{k}-\mathbf{k}'}\delta_{\sigma\sigma'})\{D(\varepsilon^{\bar{\mu}}_{\mathbf{k}} + \varepsilon^{\bar{\mu}}_{\mathbf{k}'+\mathbf{q}} - \varepsilon^{\bar{\mu}}_{\mathbf{k}'} - \varepsilon^{\bar{\mu}}_{\mathbf{k+q}})(n^{\bar{\mu}}_{\sigma'\mathbf{k}'} - n^{\bar{\mu}}_{\sigma'\mathbf{k}'+\mathbf{q}})p^{*}_{\sigma\mathbf{k+q}}p_{\sigma\mathbf{k}} + \text{c.c.}\}\\
&+ \frac{1}{\hbar}\sum_{\sigma'\mathbf{k}'\mathbf{q}} W_{\mathbf{q}}W_{\mathbf{k}-\mathbf{k}'}\delta_{\sigma\sigma'}\{D(\varepsilon^{\mu}_{\mathbf{k+q}} + \varepsilon^{\bar{\mu}}_{\mathbf{k}} - \varepsilon^{\bar{\mu}}_{\mathbf{k}'} - \varepsilon^{\mu}_{\mathbf{k}'+\mathbf{q}})[(n^{\mu}_{\sigma\mathbf{k+q}} - n^{\mu}_{\sigma'\mathbf{k}'+\mathbf{q}})p^{*}_{\sigma'\mathbf{k}'}p_{\sigma\mathbf{k}} + (n^{\bar{\mu}}_{\sigma'\mathbf{k}'} - n^{\mu}_{\sigma\mathbf{k+q}})p^{*}_{\sigma'\mathbf{k}'+\mathbf{q}}p_{\sigma\mathbf{k}}] + \text{c.c.}\}\\
&+ \frac{1}{\hbar}\sum_{\sigma'\mathbf{k}'\mathbf{q}} W_{\mathbf{q}}W_{\mathbf{k}-\mathbf{k}'}\delta_{\sigma\sigma'}\{D(\varepsilon^{\mu}_{\mathbf{k}'} + \varepsilon^{\bar{\mu}}_{\mathbf{k}'+\mathbf{q}} - \varepsilon^{\bar{\mu}}_{\mathbf{k+q}} - \varepsilon^{\mu}_{\mathbf{k}})[(n^{\mu}_{\sigma'\mathbf{k}'} - n^{\mu}_{\sigma\mathbf{k}})p^{*}_{\sigma\mathbf{k+q}}p_{\sigma'\mathbf{k}'+\mathbf{q}} + (n^{\mu}_{\sigma\mathbf{k}} - n^{\bar{\mu}}_{\sigma'\mathbf{k}'+\mathbf{q}})p^{*}_{\sigma\mathbf{k+q}}p_{\sigma'\mathbf{k}'}] + \text{c.c.}\},\end{aligned} \tag{A4}$$

$$\begin{aligned}\left.\frac{d}{dt}p_{\sigma\mathbf{k}}\right|_{c\text{-}c} = {}& \frac{1}{\hbar}\sum_{\mu\sigma'\mathbf{k}'\mathbf{q}} W_{\mathbf{q}}(W_{\mathbf{q}} - W_{\mathbf{k}-\mathbf{k}'}\delta_{\sigma\sigma'})D(\varepsilon^{\mu}_{\mathbf{k+q}} + \varepsilon^{\mu}_{\mathbf{k}'} - \varepsilon^{\mu}_{\mathbf{k}'+\mathbf{q}} - \varepsilon^{\mu}_{\mathbf{k}})\\
&\times\{n^{\mu}_{\sigma'\mathbf{k}'}(1 - n^{\mu}_{\sigma\mathbf{k}})(1 - n^{\mu}_{\sigma'\mathbf{k}'+\mathbf{q}}) + n^{\mu}_{\sigma\mathbf{k}}n^{\mu}_{\sigma'\mathbf{k}'+\mathbf{q}}(1 - n^{\mu}_{\sigma'\mathbf{k}'}) - p^{*}_{\sigma'\mathbf{k}'+\mathbf{q}}p_{\sigma'\mathbf{k}'}\}p_{\sigma\mathbf{k+q}}\\
&+ \frac{1}{\hbar}\sum_{\mu\sigma'\mathbf{k}'\mathbf{q}} W^2_{\mathbf{q}}D(\varepsilon^{\mu}_{\mathbf{k+q}} + \varepsilon^{\bar{\mu}}_{\mathbf{k}'+\mathbf{q}} - \varepsilon^{\bar{\mu}}_{\mathbf{k}'} - \varepsilon^{\mu}_{\mathbf{k}})\{n^{\bar{\mu}}_{\sigma'\mathbf{k}'+\mathbf{q}}(1 - n^{\mu}_{\sigma\mathbf{k}})(1 - n^{\bar{\mu}}_{\sigma'\mathbf{k}'}) + n^{\mu}_{\sigma\mathbf{k}}n^{\bar{\mu}}_{\sigma'\mathbf{k}'}(1 - n^{\bar{\mu}}_{\sigma'\mathbf{k}'+\mathbf{q}}) - p^{*}_{\sigma'\mathbf{k}'}p_{\sigma'\mathbf{k}'+\mathbf{q}}\}p_{\sigma\mathbf{k+q}}\\
&- \frac{1}{\hbar}\sum_{\mu\sigma'\mathbf{k}'\mathbf{q}} W_{\mathbf{q}}(W_{\mathbf{q}} - W_{\mathbf{k}-\mathbf{k}'}\delta_{\sigma\sigma'})D(\varepsilon^{\mu}_{\mathbf{k}} + \varepsilon^{\mu}_{\mathbf{k}'+\mathbf{q}} - \varepsilon^{\mu}_{\mathbf{k}'} - \varepsilon^{\mu}_{\mathbf{k+q}})\\
&\times\{n^{\mu}_{\sigma'\mathbf{k}'+\mathbf{q}}(1 - n^{\mu}_{\sigma\mathbf{k+q}})(1 - n^{\mu}_{\sigma'\mathbf{k}'}) + n^{\mu}_{\sigma\mathbf{k+q}}n^{\mu}_{\sigma'\mathbf{k}'}(1 - n^{\mu}_{\sigma'\mathbf{k}'+\mathbf{q}}) - p^{*}_{\sigma'\mathbf{k}'}p_{\sigma'\mathbf{k}'+\mathbf{q}}\}p_{\sigma\mathbf{k}}\\
&- \frac{1}{\hbar}\sum_{\mu\sigma'\mathbf{k}'\mathbf{q}} W^2_{\mathbf{q}}D(\varepsilon^{\mu}_{\mathbf{k}} + \varepsilon^{\bar{\mu}}_{\mathbf{k}'} - \varepsilon^{\bar{\mu}}_{\mathbf{k}'+\mathbf{q}} - \varepsilon^{\mu}_{\mathbf{k+q}})\{n^{\bar{\mu}}_{\sigma'\mathbf{k}'}(1 - n^{\mu}_{\sigma\mathbf{k+q}})(1 - n^{\bar{\mu}}_{\sigma'\mathbf{k}'+\mathbf{q}}) + n^{\mu}_{\sigma\mathbf{k+q}}n^{\bar{\mu}}_{\sigma'\mathbf{k}'+\mathbf{q}}(1 - n^{\bar{\mu}}_{\sigma'\mathbf{k}'}) - p^{*}_{\sigma'\mathbf{k}'+\mathbf{q}}p_{\sigma'\mathbf{k}'}\}p_{\sigma\mathbf{k}}\end{aligned}$$

$$-\frac{1}{\hbar}\sum_{\mu\sigma'\mathbf{k}'\mathbf{q}} W_{\mathbf{q}}W_{\mathbf{k}-\mathbf{k}'}\delta_{\sigma\sigma'}D(\varepsilon^{\mu}_{\mathbf{k}}+\varepsilon^{\bar{\mu}}_{\mathbf{k}+\mathbf{q}}-\varepsilon^{\bar{\mu}}_{\mathbf{k}'+\mathbf{q}}-\varepsilon^{\mu}_{\mathbf{k}'})(p^{*}_{\sigma'\mathbf{k}'+\mathbf{q}}-p^{*}_{\sigma'\mathbf{k}'})p_{\sigma\mathbf{k}}p_{\sigma\mathbf{k}+\mathbf{q}}$$

$$-\frac{1}{\hbar}\sum_{\mu\sigma'\mathbf{k}'\mathbf{q}} W_{\mathbf{q}}W_{\mathbf{k}-\mathbf{k}'}\delta_{\sigma\sigma'}D(\varepsilon^{\mu}_{\mathbf{k}'+\mathbf{q}}+\varepsilon^{\bar{\mu}}_{\mathbf{k}'}-\varepsilon^{\bar{\mu}}_{\mathbf{k}}-\varepsilon^{\mu}_{\mathbf{k}+\mathbf{q}})\{[(1-n^{\bar{\mu}}_{\sigma\mathbf{k}})(1-n^{\mu}_{\sigma\mathbf{k}+\mathbf{q}})n^{\mu}_{\sigma'\mathbf{k}'+\mathbf{q}}+n^{\mu}_{\sigma\mathbf{k}+\mathbf{q}}n^{\bar{\mu}}_{\sigma\mathbf{k}}(1-n^{\mu}_{\sigma'\mathbf{k}'+\mathbf{q}})]p_{\sigma'\mathbf{k}'}$$

$$-[(1-n^{\bar{\mu}}_{\sigma\mathbf{k}})(1-n^{\mu}_{\sigma\mathbf{k}+\mathbf{q}})n^{\bar{\mu}}_{\sigma'\mathbf{k}'}+n^{\mu}_{\sigma\mathbf{k}+\mathbf{q}}n^{\bar{\mu}}_{\sigma\mathbf{k}}(1-n^{\bar{\mu}}_{\sigma'\mathbf{k}'})]p_{\sigma'\mathbf{k}'+\mathbf{q}}\}, \tag{A5}$$

where $W_{\mathbf{q}}$ is the statically screened Coulomb potential, which is determined by solving the Lindhard equation

$$W_{\mathbf{q}}=\frac{V_{\mathbf{q}}}{\epsilon(\mathbf{q},\omega=0)}=V_{\mathbf{q}}\Bigg/\left(1-V_{\mathbf{q}}\sum_{\mu,\sigma\mathbf{k}}\frac{n^{\mu}_{\sigma\mathbf{k}-\mathbf{q}}-n^{\mu}_{\sigma\mathbf{k}}}{\varepsilon^{\mu}_{\sigma\mathbf{k}-\mathbf{q}}-\varepsilon^{\mu}_{\sigma\mathbf{k}}}\right). \tag{A6}$$

In order to avoid divergencies that may arise when the static Lindhard equation is solved with nonequilibrium distributions, we use quasiequilibrium thermal distribution functions when evaluating Eq. (A6). Since the time-dependent thermal distributions are chosen to have the same density and kinetic energy as the actual distribution, this procedure should lead to results of reasonable accuracy.

2. Quantum-kinetic analysis of the collision contributions

The carrier-phonon and the carrier-carrier interactions are treated in the framework of nonequilibrium Green's functions. In this approach, the collision terms are determined by[30,42]

$$\left.\frac{\partial}{\partial t}G^{s<}_{b_1b_2\mathbf{k}}(t,t)\right|_{\mathrm{coll}}=-\frac{i}{\hbar}\sum_{b_3}\int_{-\infty}^{t}dt'[\sigma^{s,>}_{b_1b_3,\mathbf{k}}(t,t')G^{s,<}_{b_3b_2,\mathbf{k}}(t',t)-\sigma^{s,<}_{b_1b_3,\mathbf{k}}(t,t')G^{s,>}_{b_3b_2,\mathbf{k}}(t',t)-G^{s,>}_{b_1b_3,\mathbf{k}}(t,t')\sigma^{s,<}_{b_3b_2,\mathbf{k}}(t',t)+G^{s,<}_{b_1b_3,\mathbf{k}}(t,t')\sigma^{s,>}_{b_3b_2,\mathbf{k}}(t',t)]. \tag{A7}$$

The self-energy σ is computed in the self-consistent GW approximation

$$\sigma^{s>,<}_{b_1b_3}(t,t')=i\hbar\sum_{\mathbf{q}}w^{<,>}_{\mathbf{q}}(t',t)G^{s>,<}_{b_1b_2,\mathbf{k}-\mathbf{q}}(t,t')+g_q^2D^{<,>}_{\mathbf{q}}(t',t)G^{s>,<}_{b_1b_2,\mathbf{k}-\mathbf{q}}(t,t'), \tag{A8}$$

where $w(t,t')$ combines the Coulomb and phonon interaction and is approximately given by

$$w^{<,>}_{\mathbf{q}}(t',t)=v^{<,>}_{\mathbf{q}}(t',t)+g_q^2D^{<,>}_{\mathbf{q}}(t',t)G^{s>,<}_{b_1b_2,\mathbf{k}-\mathbf{q}}(t,t'), \tag{A9}$$

with the screened Coulomb potential v and the Fröhlich interaction matrix element g_q^2. D denotes the unperturbed LO-phonon propagators

$$D^{<}_{\mathbf{q}}(t',t)=-i\sum_{\pm}N^{\pm}_{q}e^{\pm i\omega_{\mathrm{LO}}(t-t')}, \tag{A10}$$

with $N^{\pm}_{q}=N_{\mathbf{q}}+\frac{1}{2}\pm\frac{1}{2}$. $N_{\mathbf{q}}$ is the thermal phonon distribution, i.e., the Bose-Einstein distribution.

The scattering terms can be rewritten as

$$\left.\frac{\partial}{\partial t}G^{s<}_{b_1b_2,\mathbf{k}}(t,t)\right|_{\mathrm{coll}}=\sum_{b_3,q}\int_{-\infty}^{t}dt'(\{[w^{>}_{-\mathbf{q}}(t,t')G^{s>}_{b_1b_3,\mathbf{k}-\mathbf{q}}(t,t')G^{s<}_{b_3b_2,\mathbf{k}}(t',t)]-[b_1\leftrightarrow b_2]^{*}\}-(\mathbf{k}\leftrightarrow\mathbf{k}-\mathbf{q},w_{-\mathbf{q}}\leftrightarrow w_{\mathbf{q}})). \tag{A11}$$

The screened Coulomb interaction is determined by[42]

$$v^{>}_{q}(t,t')=V_{q}\left[\int_{-\infty}^{t}dt_1L^{r}_{q}(t,t_1)w^{>}_{q}(t_1,t')+\int_{-\infty}^{t'}dt_1L^{>}_{q}(t,t_1)\times[v^{a}_{q}(t_1,t')+V_q\delta(t_1-t')]\right] \tag{A12}$$

with the polarization function $L_q=-i\hbar\Sigma_{b_1b_2,s,k}G^{>}_{b_1b_2,k}\times G^{<}_{b_2b_1,k-q}$. In the short-time regime, the screening of the Coulomb potential can be neglected, i.e., one can approximate[43] $V^{r,a}_{q}(t,t')\approx V_q\delta(t-t')$. This approximation is justified for times up to about the inverse plasma frequency $\omega_{\mathrm{pl}}^{-1}$, which is the characteristic time scale that determines the buildup of screening.[38,39] In this approximation, the screened Coulomb interaction is given by

$$v^{>}_{q}(t,t')=V_q^2L^{>}_{q}(t,t'). \tag{A13}$$

To calculate the Green's functions $G^{>,<}$, we use the generalized Kadanoff-Baym ansatz $G^{>}=G^{r}\rho$, with the retarded Green's function $G^{r}_{b_1b_2,\mathbf{k}}(t,t')\simeq-\frac{i}{\hbar}\delta_{b_1b_2}\Theta(t-t')e^{-(i/\hbar)\varepsilon_{b_1,\mathbf{k}}(t-t')}$ and the density matrix ρ whose diagonal components are the electron and hole populations n^{e} and n^{h} and whose off-diagonals are given by the polarizations p and p^{*}.

APPENDIX B: COHERENT CURRENTS ARISING IN THIRD ORDER IN THE LIGHT-MATTER INTERACTION

Here, we present a set of equations that describes the coherent generation of currents, i.e., carrier distributions that are asymmetric in k space, up to third order in the optical field. For clarity, the collision contributions (see Appendix A) are not considered.

We assume that before the optical excitation, the semiconductor is in its ground state. Denoting the order in the field by upper indices $^{(i)}$, we thus start with $n^{e(0)}_{\sigma\mathbf{k}}=n^{h(0)}_{\sigma\mathbf{k}}=p^{(0)}_{\sigma\mathbf{k}}=0$. In first order, in the light-matter interaction interband polarizations are generated according to

$$\frac{d}{dt}p^{(1)}_{\sigma\mathbf{k}}=-\frac{i}{\hbar}(\varepsilon^{e}_{\sigma\mathbf{k}}+\varepsilon^{h}_{\sigma\mathbf{k}})p^{(1)}_{\sigma\mathbf{k}}+\frac{i}{\hbar}\sum_{\mathbf{q}\neq 0}V_{\mathbf{q}}p^{(1)}_{\sigma\mathbf{k+q}}+\frac{i}{\hbar}e\mathbf{r}^{cv}_{\sigma\sigma\mathbf{k}}\cdot\mathbf{E}(t). \tag{B1}$$

Equation (B1) shows that $p^{(1)}_{\sigma\mathbf{k}}$ is induced by the optical field times the interband dipole matrix element. The coupling of all transitions in k space due to the Coulomb interaction gives rise to excitonic effects.

In second order, one can either generate carrier populations by interband excitations or one can create interband polarizations by intraband excitations, i.e.,

$$\frac{d}{dt}n^{e(2)}_{\sigma\mathbf{k}}=\frac{d}{dt}n^{h(2)}_{\sigma\mathbf{k}}=-2\,\mathrm{Im}\left(\frac{1}{\hbar}\left[e\mathbf{r}^{cv}_{\sigma\sigma\mathbf{k}}\cdot\mathbf{E}(t)+\sum_{\mathbf{q}\neq 0}V_{\mathbf{q}}p^{(1)}_{\sigma\mathbf{k+q}}\right]p^{(1)*}_{\sigma\mathbf{k}}\right), \tag{B2}$$

$$\frac{d}{dt}p^{(2)}_{\sigma\mathbf{k}}=-\frac{i}{\hbar}(\varepsilon^{e}_{\sigma\mathbf{k}}+\varepsilon^{h}_{\sigma\mathbf{k}})p^{(2)}_{\sigma\mathbf{k}}+\frac{i}{\hbar}\sum_{\mathbf{q}\neq 0}V_{\mathbf{q}}p^{(2)}_{\sigma\mathbf{k+q}}-\frac{e}{\hbar}\mathbf{E}(t)\cdot\nabla_{\mathbf{k}}p^{(1)}_{\sigma\mathbf{k}}. \tag{B3}$$

If $\mathbf{r}^{cv}_{\sigma\sigma\mathbf{k}}$ is symmetric in k space, $p^{(1)}_{\sigma\mathbf{k}}$, $n^{e(2)}_{\sigma\mathbf{k}}$, and $n^{h(2)}_{\sigma\mathbf{k}}$ are symmetric in k space since these terms are solely induced by interband excitations. Consequently, in this case the second-order populations carry no current. For a symmetric $p^{(1)}_{\sigma\mathbf{k}}$, however, the intraband excitations proportional to $\mathbf{E}(t)\cdot\nabla_{\mathbf{k}}p^{(1)}_{\sigma\mathbf{k}}$, see Eq. (B3), generate an antisymmetric second-order polarization $p^{(2)}_{\sigma\mathbf{k}}$.

In third order one can again generate carrier populations and interband polarizations. Since the charge and spin currents are determined by the populations, only their equations of motion are given,

$$\frac{d}{dt}n^{e/h(3)}_{\sigma\mathbf{k}}=-2\,\mathrm{Im}\left(\frac{1}{\hbar}\left[e\mathbf{r}^{cv}_{\sigma\sigma\mathbf{k}}\cdot\mathbf{E}(t)+\sum_{\mathbf{q}\neq 0}V_{\mathbf{q}}p^{(1)}_{\sigma\mathbf{k+q}}\right]p^{(2)*}_{\sigma\mathbf{k}}+\frac{1}{\hbar}\sum_{\mathbf{q}\neq 0}V_{\mathbf{q}}p^{(2)}_{\sigma\mathbf{k+q}}p^{(1)*}_{\sigma\mathbf{k}}\right)-\frac{e}{\hbar}\mathbf{E}(t)\cdot\nabla_{\mathbf{k}}n^{e/h(2)}_{\sigma\mathbf{k}}. \tag{B4}$$

The third-order populations are generated either by interband excitations from the second-order polarization $p^{(2)}_{\sigma\mathbf{k}}$ or by intraband excitations from the second-order populations $n^{e/h(2)}_{\sigma\mathbf{k}}$. Therefore, the creation of $n^{e/h(3)}_{\sigma\mathbf{k}}$ involves two interband and one intraband excitation. If $\mathbf{r}^{cv}_{\sigma\sigma\mathbf{k}}$ is symmetric in k space, $n^{e/h(3)}_{\sigma\mathbf{k}}$ is antisymmetric and thus corresponds to a finite current.

[1] E. Dupont, P. B. Corkum, H. C. Liu, M. Buchanan, and Z. R. Wasilewski, Phys. Rev. Lett. **74**, 3596 (1995).
[2] R. Atanasov, A. Haché, J. L. P. Hughes, H. M. van Driel, and J. E. Sipe, Phys. Rev. Lett. **76**, 1703 (1996).
[3] A. Haché, Y. Kostoulas, R. Atanasov, J. L. P. Hughes, J. E. Sipe, and H. M. van Driel, Phys. Rev. Lett. **78**, 306 (1997).
[4] R. D. R. Bhat and J. E. Sipe, Phys. Rev. Lett. **85**, 5432 (2000).
[5] P. Král and J. E. Sipe, Phys. Rev. B **61**, 5381 (2000).
[6] J. Stippler, C. Schlichenmaier, A. Knorr, T. Meier, M. Lindberg, P. Thomas, and S. W. Koch, Phys. Status Solidi B **221**, 379 (2000).
[7] C. Schlichenmaier, I. Varga, T. Meier, P. Thomas, and S. W. Koch, Phys. Rev. B **65**, 085306 (2002).
[8] M. J. Stevens, A. L. Smirl, R. D. R. Bhat, A. Najmaie, J. E. Sipe, and H. M. van Driel, Phys. Rev. Lett. **90**, 136603 (2003).
[9] J. Hübner, W. W. Rühle, M. Klude, D. Hommel, R. D. R. Bhat, J. E. Sipe, and H. M. van Driel, Phys. Rev. Lett. **90**, 216601 (2003).
[10] M. J. Stevens, A. Najmaie, R. D. R. Bhat, J. E. Sipe, and H. M. van Driel, J. Appl. Phys. **94**, 4999 (2003).
[11] A. Najmaie, R. D. R. Bhat, and J. E. Sipe, Phys. Rev. B **68**, 165348 (2003).
[12] T. M. Fortier, P. A. Roos, D. J. Jones, S. T. Cundiff, R. D. R. Bhat, and J. E. Sipe, Phys. Rev. Lett. **92**, 147403 (2004).
[13] D. H. Marti, M.-A. Dupertuis, and B. Deveaud, Phys. Rev. B **69**, 035335 (2004).
[14] R. D. R. Bhat and J. E. Sipe, Phys. Rev. B **72**, 075205 (2005).
[15] D. H. Marti, M.-A. Dupertuis, and B. Deveaud, Phys. Rev. B **72**, 075357 (2005).
[16] H. T. Duc, T. Meier, and S. W. Koch, Phys. Rev. Lett. **95**, 086606 (2005).
[17] H. Zhao, E. J. Loren, H. M. van Driel, and A. L. Smirl, Phys. Rev. Lett. **96**, 246601 (2006).
[18] S. W. Wolf, D. D. Awschalom, R. A. Buhrman, J. M. Daughton, S. von Molnar, M. L. Roukes, A. Y. Chtchelkanova, and D. M. Treger, Science **294**, 1488 (2001).
[19] I. Žutić, J. Fabian, and S. Das Sarma, Rev. Mod. Phys. **76**, 323 (2004).
[20] I. Rumyantsev, A. Najmaie, R. D. R. Bhat, and J. E. Sipe, in *International Quantum Electronics Conference 2004* (IEEE, Piscataway, NJ, 2004), pp. 486–487.
[21] M. W. Wu and C. Z. Ning, Phys. Status Solidi B **222**, 523 (2000); Eur. Phys. J. B **18**, 373 (2000).
[22] J. Kainz, U. Rössler, and R. Winkler, Phys. Rev. B **70**, 195322 (2004).
[23] S. Pfalz, R. Winkler, T. Nowitzki, D. Reuter, A. D. Wieck, D. Hägele, and M. Oestreich, Phys. Rev. B **71**, 165305 (2005).
[24] I. D'Amico and G. Vignale, Phys. Rev. B **62**, 4853 (2000); Phys. Rev. B **65**, 085109 (2002).
[25] H. Haug and S. W. Koch, *Quantum Theory of the Optical and*

Electronic Properties of Semiconductors, 4th ed. (World Scientific, Singapore, 2004).

[26] W. Schäfer and M. Wegener, *Semiconductor Optics and Transport Phenomena* (Springer, Berlin, 2002).

[27] M. Lindberg and S. W. Koch, Phys. Rev. B **38**, 3342 (1988).

[28] W. Schäfer, J. Opt. Soc. Am. B **13**, 1291 (1996).

[29] T. Meier, C. Sieh, S. W. Koch, Y.-S. Lee, T. B. Norris, F. Jahnke, G. Khitrova, and H. M. Gibbs, *Nonlinear Optical Properties of Semiconductor Quantum Wells Inside Microcavities*, in *Optical Microcavities*, edited by K. Vahala (World Scientific, Singapore, 2004).

[30] H. Haug and A.-P. Jauho, *Quantum Kinetics in Transport and Optics of Semiconductors* (Springer, Berlin, 1998).

[31] T. Meier, G. von Plessen, P. Thomas, and S. W. Koch, Phys. Rev. Lett. **73**, 902 (1994).

[32] F. Rossi, T. Meier, P. Thomas, S. W. Koch, P. E. Selbmann, and E. Molinari Phys. Rev. B **51**, 16943 (1995).

[33] T. Meier, F. Rossi, P. Thomas, and S. W. Koch, Phys. Rev. Lett. **75**, 2558 (1995).

[34] T. Meier, P. Thomas, and S. W. Koch, *Coherent Dynamics of Photoexcited Semiconductor Superlattices with Applied Homogeneous Electric Fields*, in *Ultrafast Phenomena in Semiconductors*, edited by K. T. Tsen (Springer, New York, 2001), pp. 1–92.

[35] E. I. Blount, Solid State Phys. **13**, 305 (1962).

[36] N. C. Constantinou and B. K. Ridley, J. Phys.: Condens. Matter **1**, 2283 (1989).

[37] P. A. Knipp and T. L. Reinecke, Phys. Rev. B **48**, 5700 (1993).

[38] R. Huber, C. Kübler, S. Tübel, A. Leitenstorfer, Q. T. Vu, H. Haug, F. Köhler, and M.-C. Amann, Phys. Rev. Lett. **94**, 027401 (2005).

[39] Q. T. Vu, H. Haug, W. A. Hügel, S. Chatterjee, and M. Wegener, Phys. Rev. Lett. **85**, 3508 (2000).

[40] P. Gartner, L. Bányai, and H. Haug, Phys. Rev. B **60**, 14234 (1999).

[41] P. Gartner, L. Bányai, and H. Haug, Phys. Rev. B **62**, 7116 (2000).

[42] L. Bányai, Q. T. Vu, B. Mieck, and H. Haug, Phys. Rev. Lett. **81**, 882 (1998).

[43] Q. T. Vu, L. Bányai, P. Tamborenea, and H. Haug, Europhys. Lett. **40**, 323 (1997).